Hydrogen Deuterium Exchange Mass Spectrometry identifies the dominant paratope in CD20 antigen binding to the NCD1.2 monoclonal antibody

Biochemical Journal (2021) **478** 99–120
https://doi.org/10.1042/BCJ20200674

PORTLAND PRESS

Research Article

Hydrogen deuterium exchange mass spectrometry identifies the dominant paratope in CD20 antigen binding to the NCD1.2 monoclonal antibody

Lukas Uhrik[1], Lenka Hernychova[1], Petr Muller[1], Umesh Kalathiya[2], Malgorzata M. Lisowska[2], Mikolaj Kocikowski[2,3], Maciej Parys[3], Jakub Faktor[2], Marta Nekulova[1], Chris Nortcliffe[4], Pavlina Zatloukalova[1], Barbara Ruetgen[5], Robin Fahraeus[1,2,6], Kathryn L. Ball[3], David J. Argyle[3], Borivoj Vojtesek[1] and Ted R. Hupp[1,2,3]

[1]Research Centre for Applied Molecular Oncology, Masaryk Memorial Cancer Institute, Zluty kopec 7, 656 53 Brno, Czech Republic; [2]International Centre for Cancer Vaccine Science, University of Gdansk, ul. Kładki 24 80-822 Gdańsk, Poland; [3]Institute of Genetics and Molecular Medicine, University of Edinburgh, EH4 2XR Edinburgh, U.K.; [4]Sciex, Phoenix House Lakeside Drive Centre Park WA1 1RX, Warrington, U.K.; [5]Clinical Pathology, Department of Pathobiology, University of Veterinary Medicine Vienna, Veterinärplatz 1, 1210 Vienna, Austria; [6]Institut de Génétique Moléculaire, INSERM Unité 940, Université Paris VII, Hôpital St Louis, Paris, France

Correspondence: Ted R. Hupp (Ted.Hupp@ed.ac.uk) or Borivoj Vojtesek (vojtesek@mou.cz) or Lenka Hernychova (lenka.hernychova@mou.cz)

A comparative canine–human therapeutics model is being developed in B-cell lymphoma through the generation of a hybridoma cell that produces a murine monoclonal antibody specific for canine CD20. The hybridoma cell produces two light chains, light chain-3, and light chain-7. However, the contribution of either light chain to the authentic full-length hybridoma derived IgG is undefined. Mass spectrometry was used to identify only one of the two light chains, light chain-7, as predominating in the full-length IgG. Gene synthesis created a recombinant murine–canine chimeric monoclonal antibody expressing light chain-7 that reconstituted the IgG binding to CD20. Using light chain-7 as a reference sequence, hydrogen deuterium exchange mass spectrometry was used to identify the dominant CDR region implicated in CD20 antigen binding. Early in the deuteration reaction, the CD20 antigen suppressed deuteration at CDR3 (V_H). In later time points, deuterium suppression occurred at CDR2 (V_H) and CDR2 (V_L), with the maintenance of the CDR3 (V_H) interaction. These data suggest that CDR3 (V_H) functions as the dominant antigen docking motif and that antibody aggregation is induced at later time points after antigen binding. These approaches define a methodology for fine mapping of CDR contacts using nested enzymatic reactions and hydrogen deuterium exchange mass spectrometry. These data support the further development of an engineered, synthetic canine–murine monoclonal antibody, focused on CDR3 (V_H), for use as a canine lymphoma therapeutic that mimics the human–murine chimeric anti-CD20 antibody Rituximab.

Introduction

Age-related diseases in humans include enhanced susceptibility to virus infections, arthritis, metabolic diseases, cognitive dysfunction, and cancer development. These pathologies are controlled, in part, by the genetic background, exposure to environmental factors, age-related epigenetic, proteomic, and genetic changes in the cell, and by the integrity of the host immune response [1]. The paucity of physiological models that could drive an understanding of these complex multi-factorial pathways *in vivo* make it quite challenging to improve the treatment of disease. 'One World Health' proposes the unification of medical and veterinary sciences to develop cross-species research into spontaneous and infectious disease pathogenesis [2,3]. Acquiring a deeper understanding of the *in vivo* function and regulation of naturally occurring spontaneous disease, for example, the changes in immunity in age-related diseases like cancer, will be important to improve animal health and welfare.

Received: 4 September 2020
Revised: 2 December 2020
Accepted: 7 December 2020

Accepted Manuscript online: 7 December 2020
Version of Record published: 13 January 2021

Biochemical Journal (2021) 478 99–120
https://doi.org/10.1042/BCJ20200674

Immunotherapeutics have emerged as a compelling treatment choice for some human cancers such as those that express CD20, CTLA-4, or the immune checkpoint axis PD1/PDL1 [4–6]. Such agents attempt to exploit, mimic, or stimulate the natural immune defenses. Additional monoclonal antibodies that are used to build on our physiological knowledge of cell signalling, target receptors including VEGF, EGFR, ERBB2, CD40, CD33, and CD52 [7]. However, unexpected physiological problems can emerge in the use of antibody therapeutics. The antibody Yervoy was reported to induce a cytokine storm in healthy humans [8]. In addition, resistance to immunotherapies can emerge [9]. This highlights the difficulty in predicting monoclonal antibody responses in human patients. One major limitation in developing monoclonal antibody therapeutics is that the host immune system in ageing and/or ill human populations have very few 'physiological' preclinical models that can be used to predict antibody efficacy. Current robust rodent models such as xenografts in immune-deficient mice do not successfully predict clinical efficacy in complex immune-competent diseases. Improved physiological and age-correlated disease models would be of high value to stimulate more innovative immunotherapeutics of benefit to a larger population of patients.

Breeds of the domestic dog *Canis lupus* suffer from many spontaneous and age-related diseases such as cancer, arthritis, and viralopathies. This offers an opportunity to develop the spontaneous canine disease as a preclinical model that better represents human disease states [10]. Spontaneous tumours in dogs share important clinical, pathological, immunologic, molecular, diagnostic, and therapeutic characteristics with corresponding human disease and may be treated with similar anti-cancer modalities as in humans. Spontaneous tumours in dogs can provide an improved and more relevant model for developing innovative cancer therapeutic concepts that are closer to man than rodent models [11,12]. For example, EGFR is emerging as a target for the development of imaging modalities that can be experimentally examined in spontaneous canine cancers [13,14]. In addition, the genetic features of spontaneous canine glioma and its similarities to paediatric and adult human glioma [15] which provides a foundation for using canine as a physiological model for the human counterpart. Evidence for how canine cancer models can drive experimental therapeutics for potential use in human cancers was shown by data highlighting that doxorubicin can be delivered to spontaneous canine brain tumuors using synthetic minicells [16]. Such innovative approaches not only aim to improve the health of this animal, but it also provides a roadmap for developing novel preclinical models for testing new modalities for use in human populations.

One of the first paradigms for the success of monoclonal antibody therapeutics in human cancer patients has been formed by an antibody that targets the CD20 receptor [17]. CD20 is a four-pass transmembrane receptor expressed in B-cells and lymphoma [17,18]. In humans, CD20 is targeted successfully with the human–mouse chimeric monoclonal antibody, Rituximab [19,20]. Additional evidence indicates that Rituximab can be used in the treatment of other diseases including arthritis [21], immune-related indications [22–24], and in transplantation [25]. There are additional antibodies used that target CD20 in humans including the 'biosimilars' [26] Ibritumomab and Tositumomab [27,28]. Although the Rituximab and chemotherapy regime (R-CHOP) has had a positive impact on patient management, there are views towards ever-improving anti-CD20 modalities mainly because up to one-third of patients suffer a degree of mild to severe toxicity using Rituximab [29]. Reducing Rituximab toxicity using novel combined treatments or improving immunological responses with this monoclonal antibody is a key aim of translational research.

Canine lymphomas have been shown to have a similar molecular signature to the human equivalent [30,31]. This provides an opportunity to develop a canine 'Rituximab mimetic' and use it to develop innovative approaches to reduce antibody toxicity using combined agents. There is currently no clinically approved anti-CD20 monoclonal antibody used for the treatment of canine lymphoma and Rituximab does not bind to the canine CD20 epitope [32]. There have been anti-CD20 mouse monoclonal antibodies developed that can target canine CD20 [33] but clinical trials have not been forthcoming. We had previously reported the development of a novel anti-CD20 murine monoclonal antibody derived from a murine hybridoma that targets canine CD20 protein [32]. The monoclonal can bind CD20 in immunohistochemical platforms and a bioactive scFV can be cloned suggesting the possibility for its development as a recombinant antibody. However, the hybridoma from which the antibody was derived produces two light chain mRNA [32], questioning its utility as a recombinant biologic. In this report, we determine whether both light chains assemble into the authentic full-length IgG produced by this anti-CD20 hybridoma; whether recombinant mouse–dog chimeric full-length IgG versions of the antibody are bioactive; and define the dominant CDR contact to drive future structure–function studies. Together, these approaches will guide this antibody's future utility as a recombinant canine-ized monoclonal antibody for developing novel combined therapeutics for the treatment of canine and human diseases.

Biochemical Journal (2021) 478 99–120
https://doi.org/10.1042/BCJ20200674

Materials and methods

General reagents

The hybridoma NCD1.2 [32] was grown in DMEM with 10% foetal bovine serum. The NCD1.2 monoclonal antibody was purified using Protein A. RNA was extracted using Trizol from the NCD1.2 hybridoma cells and reverse transcription (Qiagen) was used to obtain cDNA. HEK293 (human embryonic kidney cells, GEO accession no. GSE119929) were obtained from ATCC and grown in DMEM plus 10% foetal bovine serum. CLBL1 [34] (dog B-cell lymphoma, GEO accession no. GSE81110) grown in IMDM plus 20% foetal bovine serum and SUDHL4 (human B-cell lymphoma, GEO accession no. GSE132365) grown in RPMI and 10% foetal bovine serum. Synthetic peptides were from Mimotopes (Australia). 5(6)-FAM was from Anaspec (AS-81002).

Flow cytometry and ELISA analyses

Flow cytometry (FCM) expression of CD20 was evaluated using FACSVerse (BD-Biosciences, Belgium). ELISA was performed using biotinylated CD20 peptide (as described [32]). Briefly, 96 well Costar plates (white, high protein binding) were coated with 100 µl of streptavidin (1 µg/ml in H_2O) overnight at 37°C. The wells were blocked with PBS containing tween-20 (0.1%) and 3% BSA (PBSTB), and the CD20 peptide was incubated at 1 µg/ml in PBSTB for 1 h to capture the peptide. The recombinant NCD1.2 monoclonal antibody or the NCD1.2 mouse IgG was titrated into the wells. Detection was performed using anti-canine IgG coupled to peroxidase for detecting the recombinant antibody containing the canine Fc (A6792, Sigma) or anti-mouse IgG (DAKO, P260) coupled to peroxidase for detecting the mouse IgG NCD1.2. The reaction was developed using ECL and read using a *PerkinElmer Fluoroskan*.

Mass spectrometry — mapping the antibody peptide fragments

In-solution digestion of the NCD1.2 monoclonal antibody

Rapigest SF powder (1 mg, Waters) was suspended in 50 mM Ammonium Bicarbonate to give a 0.2% (w/v) solution. It was used for dilution of the anti-CD20 canine monoclonal antibody (NCD1.2) in a final ratio of 1 : 1 (v/v, Rapigest : NCD1.2) to give 0.1% Rapigest solution and 1 mg/ml for the final concentration of NCD1.2. The sample was heated at 90°C for 5 min and then cooled to room temperature and shortly centrifuged. The reduction in the di-sulfide bonds of the antibody was performed using DTT (final concentration 5 mM) by incubating at 60°C for 30 min. After cooling, the cysteines were alkylated using iodoacetamide (final concentration 15 mM) in the dark for 30 min. DTT was added again in the same concentration to reduce over-alkylation and the sample was incubated at room temperature for 15 min. Proteins were enzymatically digested overnight at 37°C using three enzymes in order to acquire the optimal peptide coverage for mapping; (1) trypsin (sequencing grade modified trypsin, Promega) in a 1 : 100 ratio (w/w) of trypsin : protein; (2) trypsin with LysC (sequencing grade, Roche) in a final ratio of 1 : 10 (w/w) LysC : protein; and (3) Pepsin (Promega) in a final ratio of 1 : 100 (w/w) pepsin : protein. The next day, the sample was centrifuged and formic acid (FA) was alternatively added to acidify the sample solution to pH 3–4 with subsequent incubation at 37°C for 45 min when Rapigest was hydrolyzed to prevent suppression of peptide ionization. The peptides were purified using Micro SpinColumns C-18 (Harvard Apparatus, U.S.A.) prior to mass spectrometry analysis.

LC–MS/MS analysis (Orbitrap Elite system)

Peptides from in-solution digestion was injected using a robotic system based on the HTS-XT platform (CTC Analytics, Zwingen, Switzerland) were trapped and desalted on-line on a peptide microtrap (Michrom Bioresources, Auburn, CA) for 3 min at flow rate 20 µl/min and eluted onto an analytical column (Jupiter C18, 1.0 × 50 mm, 5 µm, 300 Å, Phenomenex, Torrance, CA) and separated using a linear gradient elution of 10% B in 2 min, followed by 31 min isocratic elution at 40% B. Solvents were: A — 0.1% FA in water, B — 80% ACN/0.08% FA. The trap cartridge and the analytical column were kept at 1°C and flow rates were directed by nano- and loading-pumps from LC-system (UltiMate 3000 RSLCnano, Thermo Scientific, Dionex, Massachusetts, U.S.A.). The mass spectrometric analysis was carried out using an Orbitrap Elite mass spectrometer (Thermo Fisher Scientific, Massachusetts, U.S.A.) with ESI ionization on-line connected with the instrument was operated in a data-dependent mode for peptide mapping (LC–MS/MS). Each MS scan was followed by MS/MS scans of the top three most intensive ions from both CID and HCD fragmentation spectra.

Biochemical Journal (2021) 478 99–120
https://doi.org/10.1042/BCJ20200674

Tandem mass spectra were searched using SequestHT against the cRap protein database (ftp://ftp.thegpm.org/fasta/cRAP) containing the sequence of the anti-CD20 antibody with the following search settings: mass tolerance for precursor ions of 10 ppm, mass tolerance for fragment ions of 0.6 Da, no enzyme specificity, two maximum missed cleavage sites and no-fixed or variable modifications were applied. The false discovery rate (FDR) at peptide identification level was set to 1%. Sequence coverage was analyzed with *Proteome Discoverer* software version 1.4 (Thermo Fisher Scientific, Massachusetts, U.S.A.).

LC–MS/MS analysis (TripleTOF 5600+ system)

Samples were separated on Eksigent Ekspert nanoLC 400 system (SCIEX, Dublin, California) liquid chromatograph. The output from the separation column was coupled to a nano-electrospray source TripleTOF 5600+ (SCIEX, Toronto, Canada). Nitrogen was used as a drying and nebulizing gas; temperature and flow of drying gas were set to 150°C and 12 psi. the capillary voltage was 2.65 kV. Peptides were trapped on a C18 PepMap100 pre-column (Thermo Fisher Scientific, U.S.A.) with a particle size 5 μm, 100 Å, 300 μm × 5 mm. A 10 min washing with a solvent consisting of 2% ACN and 0.05% TFA (v/v) was followed by peptide elution into an analytical column. The analytical separation was performed on a PicoTip emitter 75 μm × 210 mm (New Objective, Woburn, U.S.A.) self-packed with ProntoSIL 120-3-C18 AQ sorbent (3 μm particles, Bischoff, Leonberg, Germany). For chromatography, the mobile phase A was composed of 0.1% FA in water (v/v), and the mobile phase B was composed of 0.1% FA in ACN (v/v). The analytical column was equilibrated first for 30 min in the buffer containing 5% mobile phase B. Peptide separation was performed using a gradient elution of peptides from 5% mobile phase B and linearly increased up to 40% mobile phase B over 120 min. A TripleTOF 5600+ mass spectrometer was operated in information-dependent mode (IDA). The TOF-MS spectrum (250 ms accumulation time) was measured in each cycle followed by collision-induced dissociation (CID) fragmentation of 15 of the most intense precursor ions and their MS/MS spectra measurement. Minimum precursor ion intensity was 100 cps, accumulation time was 75 ms and cycle time of IDA method was 1425 ms. Shotgun data were searched using *ProteinPilot*™ version 5.0.1 (SCIEX, Canada) against the custom-made reference protein database with the sequence of the anti-CD20 antibody. *ProteinPilot*™ 5.0.1 settings were as follows: digestion criteria were set with the agent as trypsin and alkylation with iodoacetamide. Samples were searched both with and without additional ID focuses of variants: Empirical Swiss-Prot, SNP-derived, Zhang Misincorporations, and amino acid substitutions. A FDR was produced with an error rate of 0.05 (5%).

Hydrogen deuterium exchange mass spectrometry

NCD1.2 IgG (1 μM final concentration) was diluted 10-fold with phosphate buffer in H_2O (75 mM Na_2HPO_4, 25 mM NaH_2PO_4, 50 mM KCl, pH 7.4) and subsequently 2-fold diluted with quench buffer (0.5 M TCEP-HCl, 4 M urea, 1 M glycine and 3 μl pepsin with concentration 1 mg/ml) that acidified the samples to pH 2.3. These samples were used for the preparation of the undeuterated control sample and for the peptide mapping. Deuterated samples used were either (i) the anti-CD20 antibody free or (ii) in complex with CD20 peptide (the biotin-SGSG-DPANPSEKNSLSIQYCGSIR-amide) incubated with 1 mM DTT overnight at 37°C before the interaction. There is one cysteine residue in the CD20 peptide used in this report (biotin-SGSG-DPANPSEKNSLSIQYCGSIR) so DTT was included to ensure the peptide epitope was not perturbed via the formation of intermolecular di-sulfide bridges). The antibody : peptide complex was mixed at a molar ratio of 1 : 10 and then preincubated in H_2O phosphate buffer for 60 min at room temperature. Exchange of deuterium was initiated by 10-fold dilution with phosphate buffer prepared in D_2O (pD 7.0) carried out at room temperature. All chemicals used for making this phosphate buffer (Na_2HPO_4, NaH_2PO_4, and KCl) were directly added to the D_2O. Deuteration was quenched at 10 s, 1 min, 10 min, and 24 h (fully deuterated control sample) by the addition quench buffer (0.5 M TCEP-HCl, 4 M urea, 1 M glycine and 3 μl pepsin with concentration 1 mg/ml) at room temperature, followed with 3 min incubation to allow pepsin to partially proteolyze the antibody, and then the sample was snap frozen in liquid nitrogen. All samples were prepared in triplicates. Blank injections were performed between each injection to confirm the absence of peptide carryover from previous runs. Peptic peptides were identified in separate LC–MS/MS analysis. Replicates and fully deuterated samples were prepared according to the recommendations introduced recently for HDX methodology [35].

Each sample was thawed and injected onto an immobilized nepenthesin-1 column (AffiPro s.r.o. CZ), 15 μl bed volume, flow rate 20 μl/min, 2% acetonitrile/0.05% TFA. Peptides were trapped and desalted on-line on a peptide microtrap (Michrom Bioresources, Auburn, CA) for 2 min at flow rate 20 μl/min. Next, the peptides were eluted onto an analytical column (Jupiter C18, 1.0 × 50 mm, 5 μm, 300 Å, PheRomenex, CA) and

separated using a 2 min linear gradient elution of 10–40% B buffer in A buffer, followed by 31 min isocratic elution at 40% B buffer. Solvents used were: A buffer — 0.1% FA in water, B buffer — 80% acetonitrile/0.08% FA. The immobilized nepenthesin-1 column, trap cartridge and the analytical column were kept at 1°C using a refrigerated system (Science Instruments and Software, s.r.o., CZ). The mass spectrometric analysis was carried out using an Orbitrap Elite mass spectrometer (Thermo Fisher Scientific, Massachusetts, U.S.A.) with ESI ionization on-line connected with a robotic system based on the HTS-XT platform (CTC Analytics, Zwingen, Switzerland). The instrument was operated in a data-dependent mode for peptide mapping (HPLC–MS/MS). Each MS scan was followed by MS/MS scans of the top three most intensive ions from both CID and HCD fragmentation spectra. Analysis of deuterated samples was done in HPLC–MS mode with ion detection in the orbital ion trap.

Tandem mass spectra were searched using SequestHT against the cRap protein database (ftp://ftp.thegpm.org/fasta/cRAP) containing the sequence of the anti-CD20 antibody with the following search settings: mass tolerance for precursor ions of 10 ppm, mass tolerance for fragment ions of 0.6 Da, no enzyme specificity, two maximum missed cleavage sites and no-fixed or variable modifications were applied. The FDR at peptide identification level was set to 1%. Sequence coverage was analyzed with *Proteome Discoverer* software version 1.4 (Thermo Fisher Scientific, Massachusetts, U.S.A.) and graphically visualized with MS Tools application [36], 95% of anti-CD20 with the light chain-7 antibody sequence was covered with 111 identified unique peptides. Analysis of deuterated samples was done in HPLC–MS mode with ion detection in the orbital ion trap. The MS raw files together with the list of peptides (peptide pool) identified with high confidence characterized by requested parameters (amino acid sequence of each peptide, its retention time, XCorr, and ion charge) were processed using *HDExaminer* version 2.2 (Sierra Analytics, Modesto, CA). The software used to analyze protein and peptide behaviour, create the uptake plots that measured peptide deuteration over time with calculated confidence level (high, medium confidence are accepted, low confidence is rejected). The average standard deviation (repeatability) was 0.067 (Supplementary Table S1). The results from the peptide pool were displayed as graph showing the evolution of deuteration at individual parts of the protein at the same time and different protein states plotted using the GraphPad Prism version 5.03 for Windows (GraphPad Software, San Diego, CA, U.S.A.). Additional web-based application named 'MS Tools' [36] was used for the creation of a graphical representation of H/D protection plots. The results from HDX analysis of the standard protein, myoglobin, are summarized in Supplementary Table S2. The mass spectrometry proteomics data have been deposited to the ProteomeXchange Consortium via the PRIDE [37] partner repository with the dataset identifier PXD018510; Username: reviewer38806@ebi.ac.uk, Password: eOgipxVu (mapping the antibody peptide fragments) and PXD018550; Username: reviewer76109@ebi.ac.uk, Password: IiYmwPfe (HDX-MS data). This data includes files for HDX, IDA-TripleTOF 5600+, and DDA analyses-Orbitrap Elite and is listed in Supplementary Table S3.

Results

Developing a reference polypeptide library based on two light chain mRNA sequences expressed by the NCD1.2 monoclonal antibody hybridoma cell

We had previously used degenerate PCR primers derived from the murine variable framework regions to clone and create a M13 scFV-phage library derived from NCD1.2 murine hybridoma cell line [32]. The scFV-phage library derived from this hybridoma was used to biopan against the canine CD20 peptide. Two different scFV light chain amino acid sequences were acquired that bind to the CD20 epitope suggesting that the variable domains can function when fused as a single chain. However, the utility of this recombinant NCD1.2 monoclonal antibody as a potential therapeutic for canine lymphoma was unclear because two different light chains were produced by the hybridoma cell. As such, we did not know whether the authentic high-affinity IgG was composed of a mixture of two light chains and/or what the proportion of each light chain might be represented in the authentic IgG. If the authentic full-length IgG was composed of two light chains, this would complicate its utility as a recombinant therapeutic monoclonal antibody in the future. In this study, we aimed to (i) define the dominant IgG light chain polypeptides produced in this NCD1.2 hybridoma cell line using mass spectrometry; (ii) use gene synthesis to validate the bioactivity of any recombinant chimeric versions of the monoclonal antibody; and (iii) then map the CDR regions using hydrogen deuterium exchange mass spectrometry implicated in antibody binding to its CD20 epitope to define its paratope.

Mass spectrometry can be used to *de novo* sequence monoclonal antibodies but this is not trivial [38]; for example, Rituximab subunits were analyzed recently using the state-of-the-art top and middle down mass

Biochemical Journal (2021) **478** 99–120
https://doi.org/10.1042/BCJ20200674

spectrometry [39]. To use mass spectrometry to identify the primary amino acid sequence of the authentic NCD1.2 monoclonal antibody, we first created a naïve reference database of both light chains. The reference protein library was derived from the original mRNA from the NCD1.2 hybridoma cell line. A common C-terminal reverse PCR primer was used to capture the common framework-4 region of the light chains (Figure 1A; (i)) and N-terminal forward PCR primers were used that capture the N-terminal framework-1 region of the light chain-3 or light chain-7 (Figure 1A; (ii) and (iii)). This amplified mRNA was sequenced to create a reference polypeptide database (Figure 1B; the underlined sequences represent the site encoded by the PCR primers). Prior to analysis using mass spectrometry, we confirmed that the authentic NCD1.2 IgG purified from the hybridoma cell can bind to canine CD20 expressed on canine lymphoma cells (Figure 1C). As reported previously [30], the NCD1.2 IgG does not bind to human CD20 (Figure 1C). This bioactive IgG was subjected to proteolysis using a range of enzymes and then the proteolytic peptides were analyzed using mass spectrometry to define the actual contribution of light chain-3 and/or light chain-7 polypeptides to the authentic IgG makeup (Figure 2).

Using mass spectrometry to define light chain expression in the NCD1.2 IgG

The homology of light chain-3 and light chain-7 is depicted in Figure 3A. The IgG was subjected to pepsinization, processed using LC–MS/MS, and spectral data were processed using *Proteome Discoverer 1.4*. This workflow led to nearly complete protein sequence coverage of light chain-7 (Figure 3B). The use of trypsin and

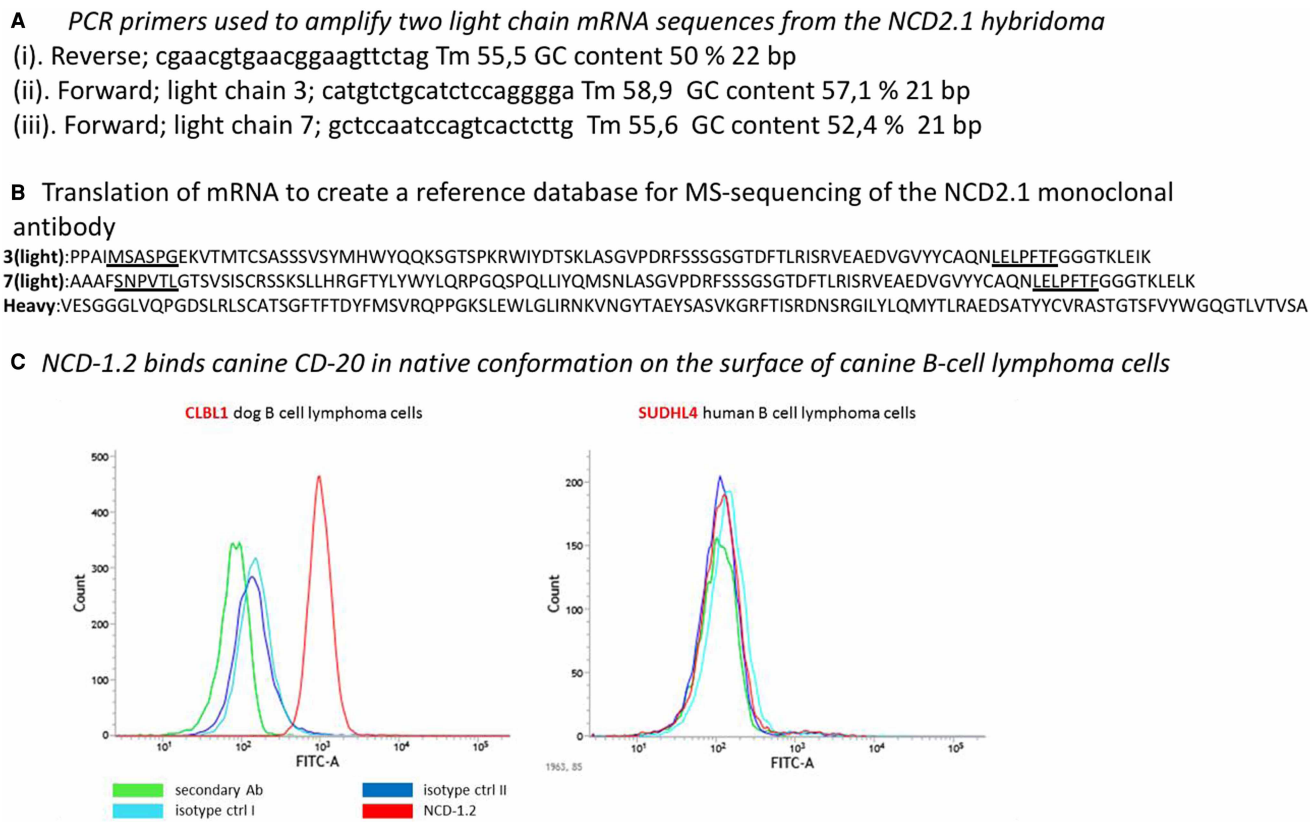

Figure 1. Primary amino acids sequence of two light chains produced by the hybridoma cell line NCD1.2.

(**A**) PCR primers were designed with homology to FR1 and FR4 of both light chain-3 and light chain-7 derived from isolated from prior scFV-phage screening. (**B**) A cDNA library was generated from the NCD1.2 hybridoma and used to PCR amplify the two variable light chain domains, sequence the PCR products, and generate the amino acid variable domain sequences as depicted; 3-light, 7-light, and heavy chain. (**C**) Flow cytometry was used to demonstrate that NCD1.2 binds to the surface of CLBL1 canine B-cell lymphoma, but not a human B-cell lymphoma cell line SUDHL4. The graphs plot cell counts (Count) as a function of fluorescence in antibody binding (FITC-A) and include the NCD1.2 IgG, isotype control II, isotype control I, and secondary antibody only.

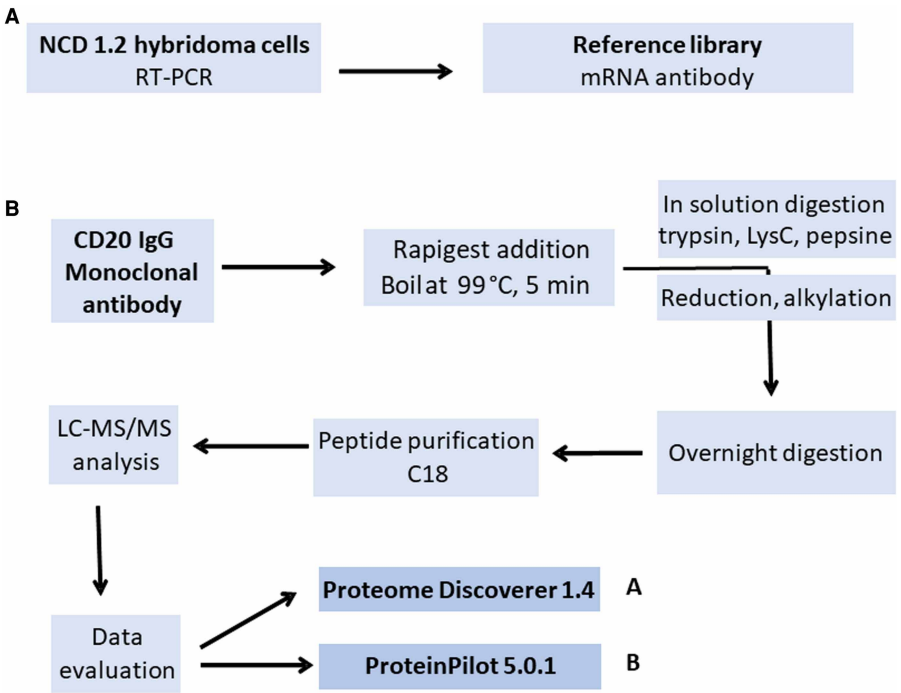

Figure 2. Workflow for defining the dominant amino acids sequences comprising the NCD1.2 monoclonal antibody.
(**A**) A polypeptide reference library was generated by sequencing the heavy chain and two light chains mRNAs from NCD1.2 hybridoma derived mRNA. (**B**) Mass spectrometric-based sequencing of the NCD1.2 IgG. The IgG was incubated with Rapigest, heated, digested with a library of enzymes to optimize peptide coverage, peptides were purified on a C-18 reverse phase column, processed using an Orbitrap Elite and TripleTOF 5600+ mass spectrometers. The data from the two mass spectrometers were evaluated using *Proteome Discoverer* 1.4 and *Protein Pilot 5.0.1*.

trypsin with LysC gave less than 40% coverage (data not shown). We did not detect any unique peptide coverage from sequences in light chain-3 (Figure 3C,D). The sequences that diverge between light chain-3 and light chain-7 reside in FR1, CDR1, FR2, and the sequence QMSN in CDR2 of light chain-7 vs DTSK in the CDR2 of light chain-3. The remaining protein sequence is identical in FR3 and CDR3 of both light chains (Figure 3A). The only missing sequence after mass spectrometric analysis in light chain-7 was Y86 in FR3 (Figure 3B–D). These data suggest that NCD1.2 IgG is composed predominately of, within our limits of detection, light chain-7.

To highlight the spectral data of light chain-7, the MS/MS spectrum of a peptide from the CDR1 of light chain-7 is shown; the HRNGFTYL, a double-charged peptide ($z = 2$) was acquired on both mass spectrometers, an Orbitrap Elite (Figure 4A) and a TripleTOF 5600+ (Figure 4B). The MS/MS spectrum of a peptide sequence from the heavy chain; the FMSWVRQPPGKSLEWLGL, a double-charged peptide with a $(M + H)^+$ 2131.1158 Da and a retention time 20.09 min, was acquired on an Orbitrap Elite (Figure 5A), and the WVRQPPGKS, a double-charged peptide ($z = 2$) with a $(M + H)^+$ 1053.5737 Da and a retention time = 52.3 min was acquired on a TripleTOF5600+ (Figure 5B). The resulting peaks in the MS/MS spectrum (Figures 4 and 5) correspond to a series of *b* and *y* ions (introduced in the table, right up in the spectrum) that resulted from CID fragmentation. Data of these peaks clearly covered the amino acid sequence of the peptide.

Although we observed no peptic coverage of light chain-3, this negative result does not allow us to conclude there is no light chain-3 peptide present in the IgG. As such we employed a different mass spectrometer to search for peptide fragments of light chain-3. The NCD1.2 IgG (1 μg/μl concentration) was trypsinized or pepsinized, alkylated and reduced, followed by processing using a 120 min LC gradient composed from 0.1% FA in water (v/v)/0.1% FA in acetonitrile (v/v) and analyzed on a Triple TOF 5600+ mass spectrometer. The instrument settings included fragmentation of top 15 precursor ions and measurement of their TOF-MS/MS spectra. Minimum precursor ion intensity was 100 cps, accumulation time per precursor was 75 ms and cycle time of

PORTLAND PRESS

Biochemical Journal (2021) **478** 99–120
https://doi.org/10.1042/BCJ20200674

A homology of light chain 3 and light chain 7

```
3 --PAIMSASPGEKVTMTCSAS------SSVSYMHWYQQKSGTSPKRWIYDTSKLASGVPD
7 AAAFSNPVTLGTSVSISCRSSKSLLHRNGFTYLYWYLQRPGQSPQLLIYQMSNLASGVPD
     . ..: * .*:::* :*      ...:*::** *:.* **:  **: *:*******

3 RFSSSGSGTDFTLRISRVEAEDVGVYYCAQNLELPFTFGGGTKLEIK
7 RFSSSGSGTDFTLRISRVEAEDVGVYYCAQNLELPFTFGGGTKLELK
  ********************************************:*
```

B

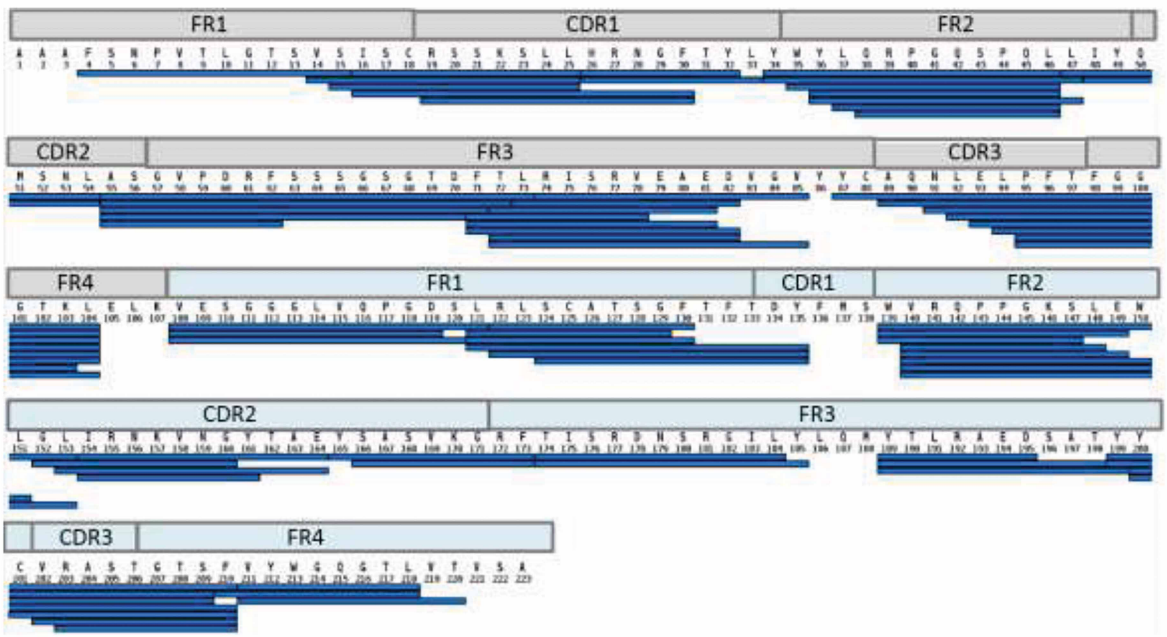

C

3(light):PPAIMSASPGEKVTMTCSASSSVSYMHWYQQKSGTSPKRWIYDTSKLASGVPDRFSSSGSGTDFTLRISRVEAEDVGVYYCAQNLELPFTFGGGTKLEIK
7(light):AAAFSNPVTLGTSVSISCRSSKSLLHRNGFTYLYWYLQRPGQSPQLLIYQMSNLASGVPDRFSSSGSGTDFTLRISRVEAEDVGVYYCAQNLELPFTFGGGTKLELK
Heavy:VESGGGLVQPGDSLRLSCATSGFTFTDYFMSWVRQPPGKSLEWLGLIRNKVNGYTAEYSASVKGRFTISRDNSRGILYLQMYTLRAEDSATYYCVRASTGTSFVYWGQGTLVTVSA

Reference light and heavy chain library from the mRNA of NCD1.2 hybridoma cells.

D

3(light):PPAIMSASPGEKVTMTCSASSSVSYMHWYQQKSGTSPKRWIYDTSKLASGVPDRFSSSGSGTDFTLRISRVEAEDVGVYYCAQNLELPFTFGGGTKLEIK
7(light):AAAFSNPVTLGTSVSISCRSSKSLLHRNGFTYLYWYLQRPGQSPQLLIYQMSNLASGVPDRFSSSGSGTDFTLRISRVEAEDVGVYYCAQNLELPFTFGGGTKLELK
Heavy:VESGGGLVQPGDSLRLSCATSGFTFTDYFMSWVRQPPGKSLEWLGLIRNKVNGYTAEYSASVKGRFTISRDNSRGILYLQMYTLRAEDSATYYCVRASTGTSFVYWGQGTLVTVSA

Peptide mapping of NCD 1.2 after pepsin digestion. The amino acid sequences not detected using mass spectrometry analysis are highlighted in red.

Figure 3. Light chain-7 peptide sequences dominate in the NCD1.2 IgG protein preparation. Part 1 of 2

(**A**) A homology alignment of light chain-3 and light chain-7, where the differences in the N-terminus extend from FR1, CDR1, FR2, and into CDR2. The identity between both light chains begins at LASGV which is at the end of CDR2 and into FR3. The data are derived from pblast (https://blast.ncbi.nlm.nih.gov) with * indicating amino acid identity, whilst ':' and '.' denoting decreasing amino acid 'similarity. (**B**) The mapping of peptic peptide fragments onto the sequence of light chain-7 and the heavy chain highlights the peptide coverage from the variable domain of the IgG. Peptides derived from light chain-3 were not identified. Using MSTools (33), the green boxes pepsin peptides. (**C**) The reference amino acid sequence library for all light chains and the heavy chain derived from NCD1.2 hybridoma cells. (**D**) A summary of the peptides not identified in this screen (in red). These sequences include Y86 in light chain-7(3), A1, A2, and A3 in light chain-7, and the final three amino acids of all FR4 chains. The result from

Figure 3. Light chain-7 peptide sequences dominate in the NCD1.2 IgG protein preparation. Part 2 of 2

the program *Proteome Discoverer* 1.4 of the anti-CD20 antibody peptide mapping (in-solution digestion with pepsin). The light chain CD20 ScFv-3 was not identified (unmarked N-part of antibody, green marked parts of amino acids were identified with high confidence, FDR threshold 0.01).

IDA method was 1425 ms. Using this methodology, we were able to map tryptic peptides (Figure 6A,C,D) or peptic peptides (Figure 6B,E,F,G) to the variable domains, with differing degrees of confidence.

The entire heavy chain amino acid sequence was identified with a high degree of confidence with *ProteinPilot* using pepsin, except for the QM sequence in FR3 (Figure 6G, in red). The entire light chain-7 sequence was also identified with a high confidence using pepsin, except for the LRI sequence in FR3 (Figure 6F). However, by comparison, the light chain-3 FR1, CDR1 FR2, and CDR2 were not identified with a high degree of confidence (Figure 6E). Using trypsin (Figure 6C,D), the mapping was not as complete as that with pepsin (Figure 6E,F), although there were more high confidence peptides mapped onto light chain-7 than that for light chain-3. Together, these data suggest that light chain-7 is the predominating light chain in the NCD1.2 IgG.

Evaluation of NCD1.2 variable domain activity as a recombinant chimeric IgG

Next, gene synthesis of the entire IgG was used as an orthogonal method to determine which light chain was bioactive when assembled as an IgG. Chimeric recombinant plasmids encoding of the light chain-3, light chain-7, and heavy chain IgG were synthesized to see if we could reconstitute activity when the heavy and light chain plasmids are expressed by co-transfection from plasmid vectors and in a non-hybridoma cell type (HEK393). The sequence of the light chain-7 and the heavy chain plasmid is shown in Figure 7A–F.

The IL2 leader sequence is from primate; the murine variable light chain was fused to the canine λ constant chain to create a murine–canine chimeric light chain; and the variable heavy chain was fused to the canine-Fc-receptor-positive canine 'B-chain' [40] to create a murine–canine chimera that would in principle be active in complement-mediated and Fcγ receptors (FcγRs)-binding mediated cell death. This feature of the Fc is based on the mouse–human chimeric antibody that targets human CD20 used in the human R-CHOP therapies (Rituximab) which induces indirect cell death via complement-mediated cell death and immunological attack from FcR-expressing innate effectors [41]. However, complement-dependent cytotoxicity (CDC) was originally thought to be the main mechanism of anti-tumour activity of Rituximab, which binds to C1q. Rituximab causes many diverse biological responses through its Fc domain, resulting in different immune response depending on the binding partner [42,43]. Cell surface transmembrane dimeric Fcγ receptors are expressed on multiple immune cells. Natural killer cells (NK) stimulated through FcγRIIIA, attack antibody opsonized targets, releasing cytolytic compounds such as granzyme B and perforin in a process called antibody-dependent cell-mediated cytotoxicity (ADCC). Additionally, binding of FcγR on phagocytic cells like macrophages, neutrophils, and monocytes leads to phagocytosis and destruction of opsonized targets, a process known as antibody-dependent cell-mediated phagocytosis (ADCP). Another mechanism stimulated through the Fc portion of Rituximab were described as 'hypercrosslinking' and include direct killing related to extracellular calcium influx and generation of reactive oxygen species. For these reasons, the canine Fc B-chain was used to capture some of the immunological benefits thought to be involved in the mouse–human chimeric antibody Rituximab effects.

The plasmid structure of light chain-7 and heavy chain chimeras are shown in Figure 7G,H. The heavy and light chains were co-transfected into HEK293 cells for 1 week, and the supernatant was measured for activity in a CD20 ELISA with anti-canine Fc HRP-conjugated secondary antibody. A titration of the light chain-7 and heavy chain reconstituted system produced detectable activity in binding to the CD20 peptide (Figure 7I). The inclusion of DTT in the ELISA ensured reduction in the single cysteine in the CD20 peptide (the biotin-SGSG-DPANPSEKNSLSIQYCGSIR) prevented inter-molecular cross-linking of the peptide (Figure 7I); there was no difference in binding to the CD20 peptide without DTT. The light chain-3 + heavy chain reconstituted assay did not result in detectable activity under these same conditions (data not shown). These data together suggest that light chain-7 forms the predominant light chain in the IgG preparation and that this chain is also the bioactive component of the hybridoma derived IgG. A parallel titration of the original NCD1.2 mouse monoclonal antibody and the recombinant canine–mouse chimera reveal a similar efficiency of

Biochemical Journal (2021) **478** 99–120
https://doi.org/10.1042/BCJ20200674

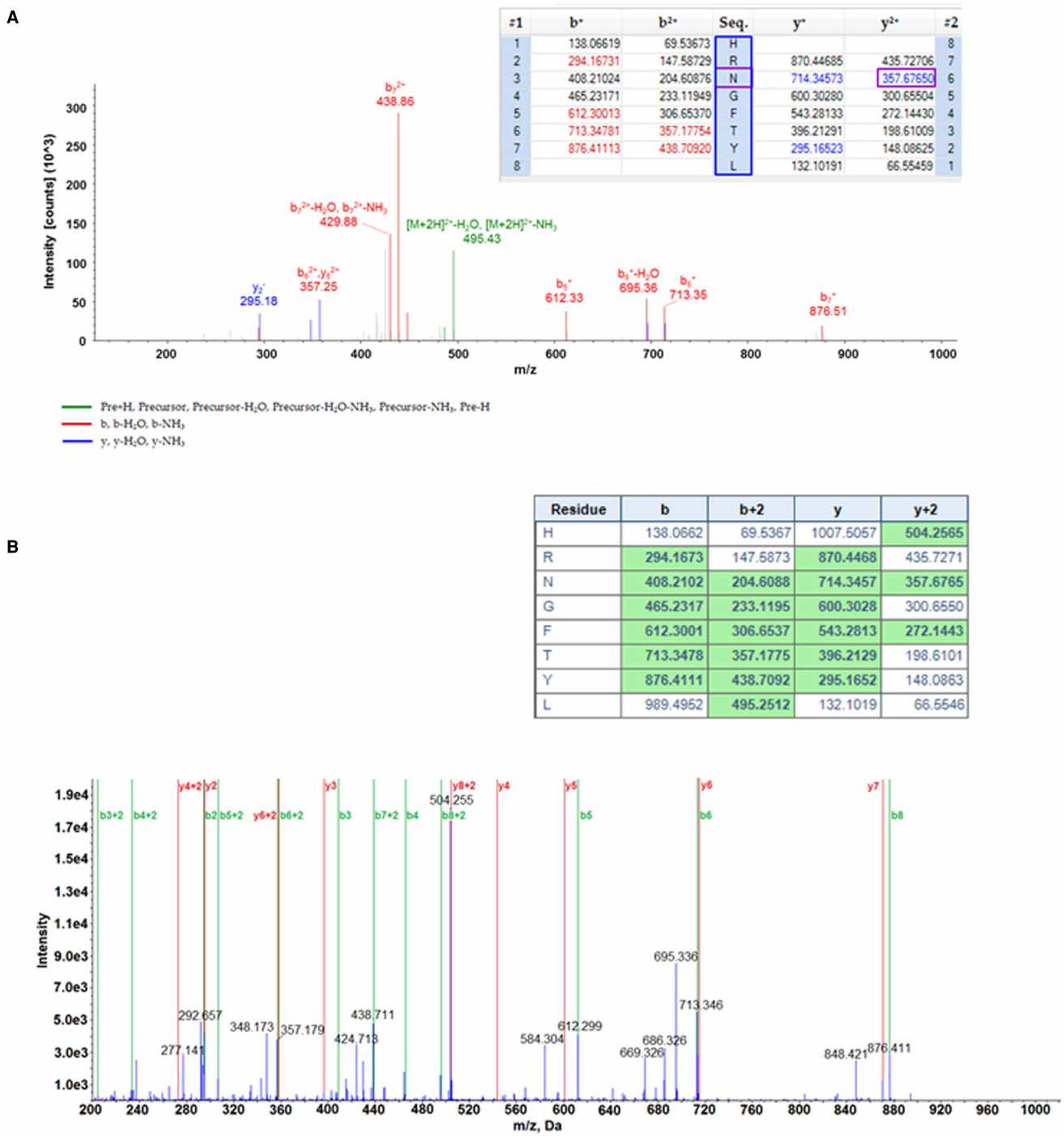

Figure 4. The MS/MS spectra of peptides derived from light chain-7 NCD1.2 monoclonal antibody.

(**A**) The HRNGFTYL double-charged ($z = 2$) peptide acquired on Orbitrap Elite and (**B**) the same peptide acquired on TripleTOF 5600+. The resulting peaks in the MS/MS spectra correspond to a series of *b* and *y* ions created from CID fragmentation. The tables show list of *m/z* fragments from spectra linked to amino acid sequences of peptides.

binding to the CD20 antigen (Supplementary Figure S1). We next mapped the CDR contacts in the IgG using hydrogen deuterium exchange mass spectrometry, using the light chain-7 sequence and heavy chain sequence as reference databases.

Biochemical Journal (2021) **478** 99–120
https://doi.org/10.1042/BCJ20200674

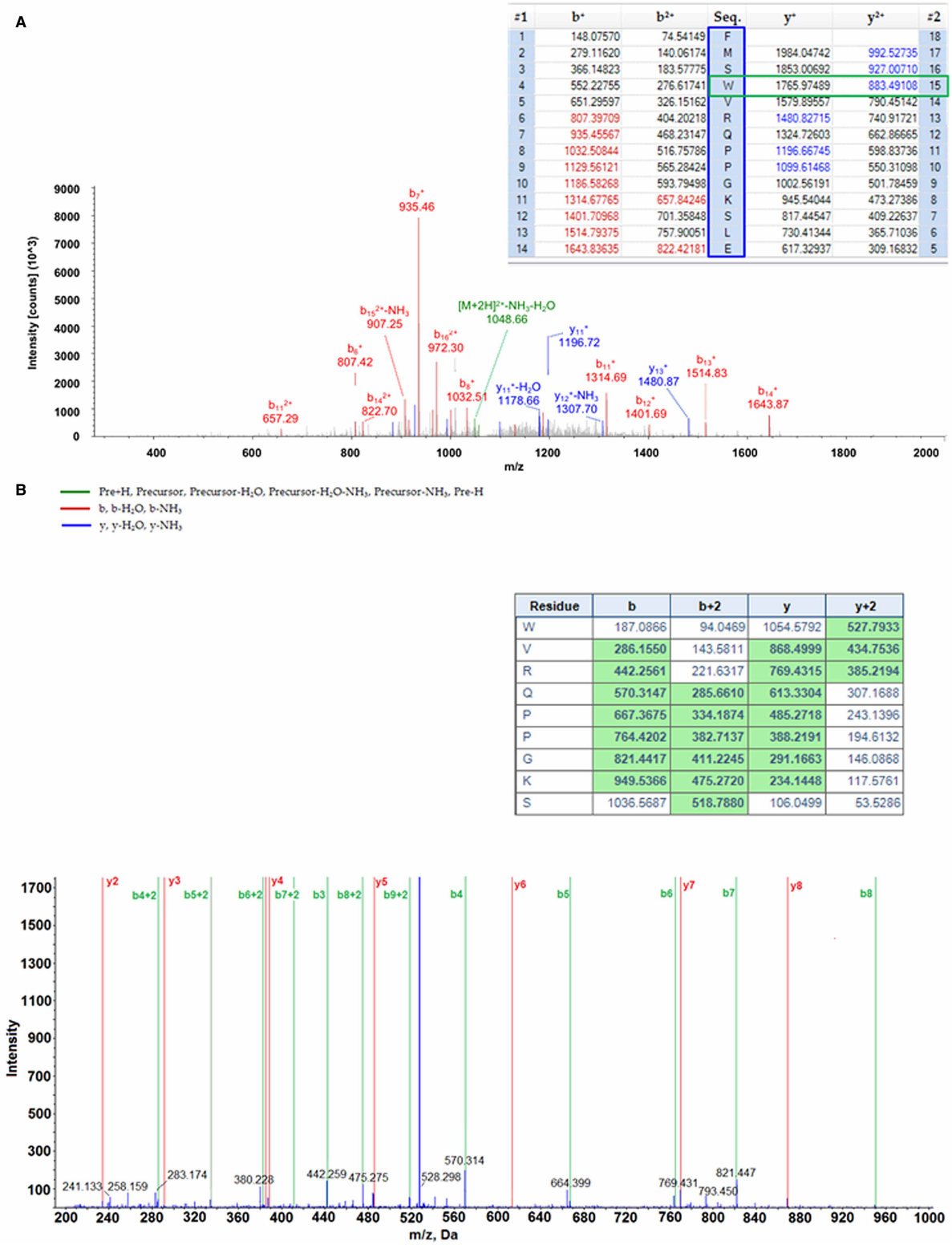

#1	b+	b2+	Seq.	y+	y2+	#2
1	148.07570	74.54149	F			18
2	279.11620	140.06174	M	1984.04742	992.52735	17
3	366.14823	183.57775	S	1853.00692	927.00710	16
4	552.22755	276.61741	W	1765.97489	883.49108	15
5	651.29597	326.15162	V	1579.89557	790.45142	14
6	807.39709	404.20218	R	1480.82715	740.91721	13
7	935.45567	468.23147	Q	1324.72603	662.86665	12
8	1032.50844	516.75786	P	1196.66745	598.83736	11
9	1129.56121	565.28424	P	1099.61468	550.31098	10
10	1186.58268	593.79498	G	1002.56191	501.78459	9
11	1314.67765	657.84246	K	945.54044	473.27386	8
12	1401.70968	701.35848	S	817.44547	409.22637	7
13	1514.79375	757.90051	L	730.41344	365.71036	6
14	1643.83635	822.42181	E	617.32937	309.16832	5

Residue	b	b+2	y	y+2
W	187.0866	94.0469	1054.5792	527.7933
V	286.1550	143.5811	868.4999	434.7536
R	442.2561	221.6317	769.4315	385.2194
Q	570.3147	285.6610	613.3304	307.1688
P	667.3675	334.1874	485.2718	243.1396
P	764.4202	382.7137	388.2191	194.6132
G	821.4417	411.2245	291.1663	146.0868
K	949.5366	475.2720	234.1448	117.5761
S	1036.5687	518.7880	106.0499	53.5286

Figure 5. The MS/MS spectra of peptides derived from heavy chain NCD1.2 monoclonal antibody.

(**A**) The FMSWVRQPPGKSLEWLGL double-charged ($z = 2$) peptide acquired on Orbitrap Elite and (**B**) the double-charged WVRQPPGKS peptide acquired on TripleTOF5600+. The resulting peaks in the MS/MS spectra correspond to a series of *b* and *y* ions created from CID fragmentation. The tables show list of *m/z* fragments from spectra linked to amino acid sequences of peptides.

Biochemical Journal (2021) **478** 99–120
https://doi.org/10.1042/BCJ20200674

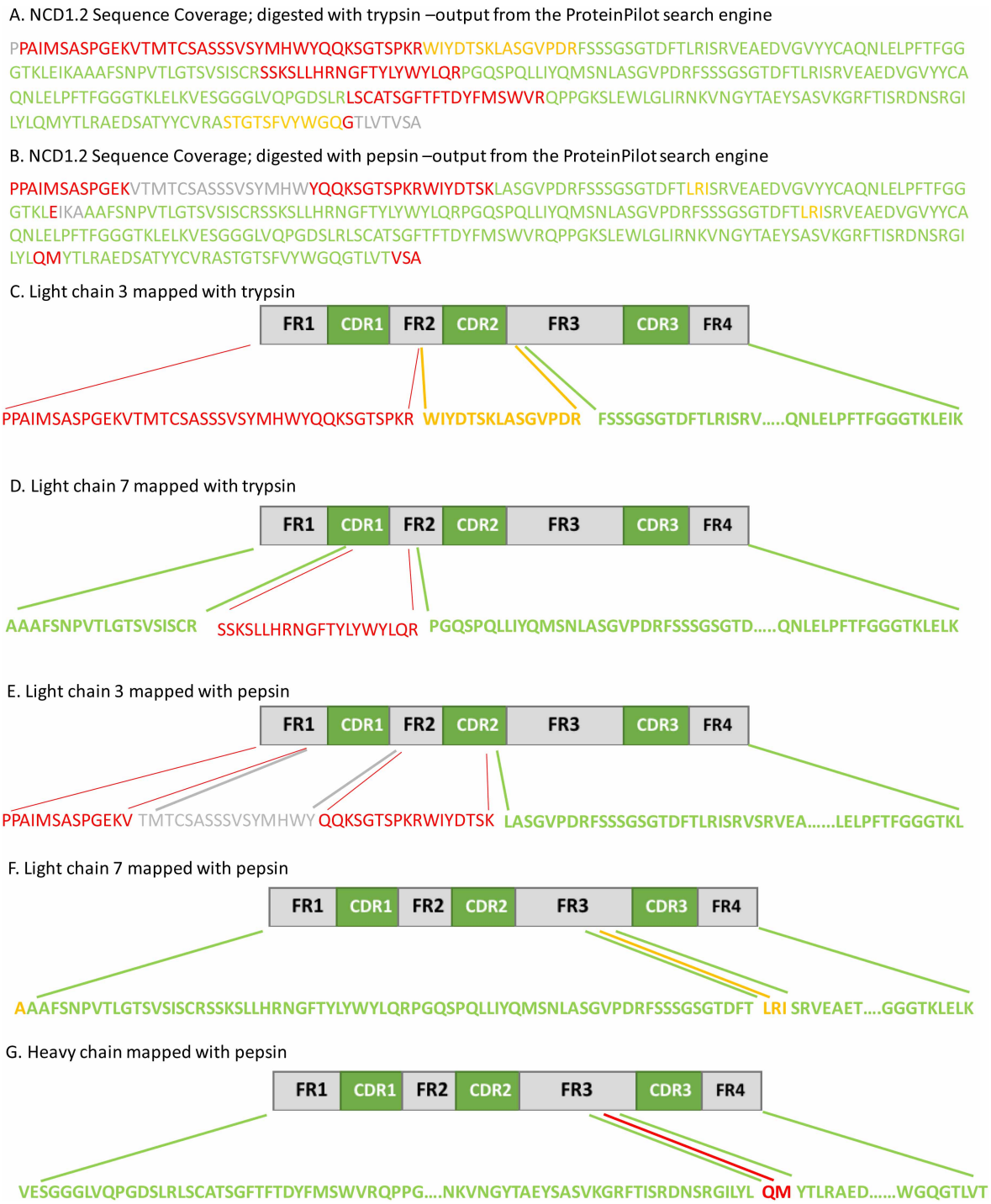

Figure 6. The LC–MS/MS peptides identified from NCD1.2 IgG using *ProteinPilot*. Part 1 of 2

NCD1.2 IgG was (**A**) trypsinized or (**B**) pepsinized and analyzed using a TripleTOF 5600+. LC–MS/MS data were searched against light chain-3 reference database in order to determine whether any light chain-3 peptides could be identified with high confidence. Output spectra were obtained and visualized in ProteinPilot™ 5.0.1 software. Output data (**A**) and (**B**) from ProteinPilot™ 5.0.1 show the peptide coverage and peptide confidence in the NCD1.2 IgG sequence. Amino acids are listed in grey were not covered by identified peptides; those in red are covered by low confidence peptides (peptide confidence ≤ 50%); those in yellow as medium confidence (peptide confidence ≤ 95% $P > 50\%$), and those in green as high confidence (peptide confidence > 95%). The *ProteinPilot*™ 5.0.1 data browser output (**A**) and (**B**) is represented as a single list of peptides that were

Figure 6. The LC–MS/MS peptides identified from NCD1.2 IgG using *ProteinPilot*. Part 2 of 2

matched to the reference sequence of Light chain-3, Light chain-7, and the Heavy chain. As such, the sequences of Light chain-3, Light chain-7, and the Heavy chain were extracted and (**C–G**) highlights the relative confidence in peptide identification; (**C**) light chain-3 peptide coverage using trypsin; (**D**) light chain-7 peptide coverage using trypsin; (**E**) light chain-3 peptide coverage using pepsin; (**F**) light chain-7 peptide coverage using pepsin; and (**G**) heavy chain peptide coverage using pepsin.

Using hydrogen deuterium exchange mass spectrometry to map the CDR contacts of the NCD1.2 IgG

Given that the light chain-7 dominates in the IgG preparation (Figure 3) and that light chain-7 can reconstitute a biochemically active antibody when co-expressed with the heavy chain as a recombinant protein in HEK293 cells (Figure 7), we used this sequence as a reference database to map the CDR contacts on the antibody when it interacts with peptide epitope. NCD1.2 IgG (1 μM final concentration) was diluted 10-fold with phosphate buffer (pH 7.4) in H_2O and subsequently 2-fold diluted with quench buffer then used in measurements as a non-deuterated control for the peptic peptide mapping. The sample was processed by acidification and proteolytic digestion with pepsin and nepenthesin-1 as described in the experimental procedures. The mock-quenched samples were measured using LC–MS/MS to determine the pepsin coverage under conditions used for hydrogen deuterium exchange mass spectrometry (Figure 8). Blue boxes highlight the antibody-derived peptides detected as a function of the amino acid sequence of the variable domains containing light chain-7 (sequence coverage was 91% with 109 unique peptides). The primary structure of light and heavy chains is also depicted together with FR (framework) and CDR (Complementarity-determining regions) regions. The light chain-7 polypeptide sequence was well represented with the digestion of both enzymes pepsin and nepenthesin-1 using the reference database (Figure 8), further affirming that the single chain-7 peptide sequence dominates the IgG preparation.

The CDR regions from the NCD1.2 antibody interacting with its' epitope peptide was next mapped using hydrogen deuterium exchange mass spectrometry. Samples of either the ligand-free NCD1.2 antibody or the NCD1.2 antibody bound to its CD20 peptide epitope (biotin-SGSG-DPANPSEKNSLSIQYCGSIR-amide) were pre-incubated in molar ratio 1 : 10 (antibody : peptide) for 60 min in H_2O phosphate buffer at room temperature. At these concentrations used, fluorescence polarization using a 5(6)-FAM labelled CD20 peptide as a tracer was used to calculate that the antibody occupancy was 98.77% (Supplementary Figure S2). Deuterium exchange was initiated by a 10-fold dilution with phosphate buffer in D_2O (pD 7.0) carried out at room temperature. Deuteration was quenched at 10 s, 1 min, and 10 min by adding the acid quench buffer at room temperature, incubating on ice for 3 min, then immediately snap-freezing in liquid nitrogen. After mass spectrometry, the data were processed using HDExaminer software to evaluate changes in deuteration of the peptides as a function of time in the absence (purple) or presence (blue) of the CD20 peptide (Figure 9). The data are plotted as % deuteration of the peptide as a function of the numbering of the amino acids 1–221 where the peptides were subjected to evaluation with HDExaminer software. The diagram highlights the positions of the CDR and FR domains from the light and heavy chain as a single polypeptide sequence of 221 amino acids for simplicity. Peptide deuteration is plotted directly above the CDR and FR domains for ease of comparison. The asterisks highlight the peptides whose deuteration was suppressed by the CD20 peptide at either of the times points. Some peptides were highly deuterated (presumably solvent exposed such as both CDR2 domains) and others less deuterated (presumably less solvent exposed such as the CDR1 domain from the light chain; Figure 9A–C). In addition, baseline deuteration generally increases in all domains over the time course from 10 to 600 s (Figure 9A–C). The results over this time course were captured in triplicate, analyzed using HDExaminer, and are summarized in Supplementary Tables S1 and S4.

One major feature in IgG deuteration rates after CD20 peptide binding was notable. At the earliest time point of deuteration (10 s), only the CDR3 (V_H) domain exhibited suppressed hydrogen deuterium exchange, suggesting that this is the dominant paratope (Figure 9A). There was no detectable binding at CDR3 (V_L) at the early or late time points (Figure 9A–C). At the 60 s time point there was additional deuterium suppression at CDR2 (V_L) (Figure 9B). By the 600 s time point, CDR3 (V_H), CDR2 (V_H), CDR2 (V_L), and CDR1 (V_L) domains exhibited decreased hydrogen deuterium exchange (Figure 9C). CDR3 (V_L), FR2 (V_L), FR3 (V_L), FR2 (V_H), and FR3 (V_H) did not exhibit suppressed hydrogen deuterium exchange, suggesting that they do not

Biochemical Journal (2021) **478** 99–120
https://doi.org/10.1042/BCJ20200674

a.IL-2 LEADER SEQUENCE (Primate)
MYRMQLLSCIALSLALVTNS
b.Murine V_L
DIVMTQAAAFSNPVTLGTSVSISCRSSKSLLHRNGFTYLYWYLQRPGQSPQLLIYQMSNLASGVPDRFSSSGSGTDFT
LRISRVEAEDVGVYYCAQNLELPFTFGGGTKLELK
c.λ light canine constant chain
QPKASPLVTLFPPSSEELGANKATLVCLISDFYPSGLKVAWKADGSTIIQGVETTKPSKQSNNKYAASSYLSLTPNKW
KSHSSFSCLVTHQGSTVEKKVAPAECS

d.IL-2 LEADER SEQUENCE (Primate)
MGWSCIILFLVATATGAHS
e.Murine V_H
EVQLVESGGGLVQPGDSLRLSCATSGFTFTDYFMSWVRQPPGKSLEWLGLIRNKVNGYTAEYSASVKGRFTISRDNSR
GILYLQMYTLRAEDSATYYCVRASTGTSFVYWGQGTLVTVGS

f. Fc constant canine chain B
ASTTAPSVFPLAPSCGSTSGSTVALACLVSGYFPEPVTVSWNSGSLTSGVHTFPSVLQSSGLYSLSSMVTVPSSRWPS
ETFTCNVAHPASKTKVDKPVLKRENGRVPRPPDCPKCPAPEMLGGPSVFIFPPKPKDTLLIARTPEVTCVVVDLDPED
PEVQISWFVDGKQMQTAKTQPREEQFNGTYRVVSVLPIGHQDWLKGKQFTCKVNNKALPSPIERTISKARGQAHQPSV
YVLPPSREELSKNTVSLTCLIKDFFPPDIDVEWQSNGQQEPESKYRTTPPQLDEDGSYFLYSKLSVDKSRWQRGDTFI
CAVMHEALHNHYTQKSLSHSPGK

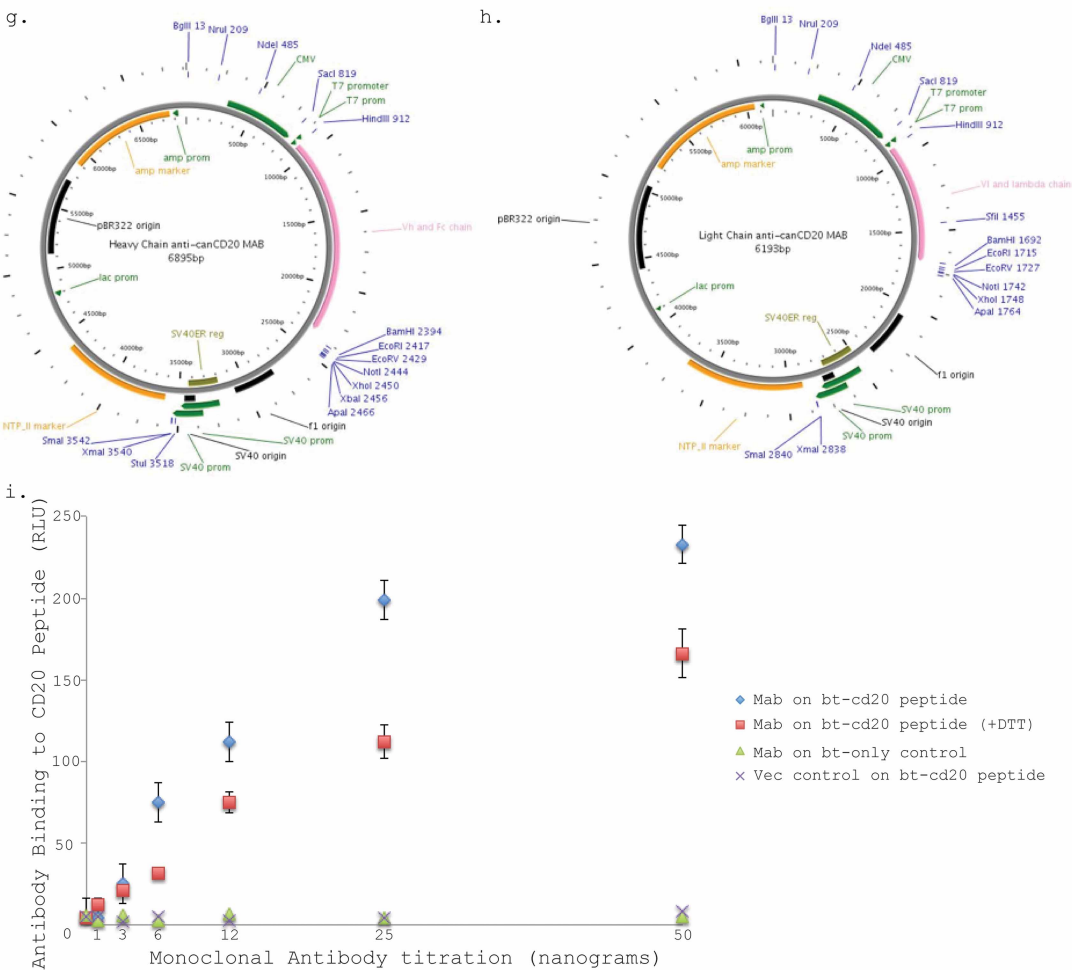

Figure 7. Bioactivity of recombinant chimeric NCD1.2 containing light chain-7. Part 1 of 2

(**A**–**F**) The sequence of the chimeric antibody is highlighted including the leader sequence, variable light chain, light constant chain, variable heavy domain, and Fc domain. The plasmid structure containing CMV promoter is highlighted in (**G**) and (**H**), and was constructed using PlasMapper [48]. (**I**) An ELISA with recombinant antibody expressed into the supernatant of HEK293 cells was used to define activity to the CD20 epitope peptide. The heavy and light chains were co-transfected into

Biochemical Journal (2021) **478** 99–120
https://doi.org/10.1042/BCJ20200674

Figure 7. Bioactivity of recombinant chimeric NCD1.2 containing light chain-7. Part 2 of 2

HEK293 cells for 1 week, and the supernatant was measured for activity in a CD20 ELISA with anti-canine Fc HRP-conjugated secondary antibody. A titration in triplicate of the light chain-7 and heavy chain reconstituted system produced detectable activity in binding to the CD20 peptide (Figure 11A). The inclusion of DTT in the ELISA ensured reduction in the cysteine in the CD20 peptide (biotin-SGSG-DPANPSEKNSLSIQYCGSIR) and precluded the formation of inter-peptide cross-links via di-sulfide bridges that might alter the epitope. The light chain-3 + heavy chain reconstituted assay did not result in detectable activity under these same conditions (data not shown). These data together suggest that light chain-7 forms the predominant light chain in the IgG preparation and that this chain is also the bioactive component of the IgG. The data are derived from triplicate titrations (with bars showing the error as a mean) with antibody binding activity (in relative light units) plotted as a function of the amount of antibody titrated (in nanograms).

comprise peptide binding sites. In fact, most FR regions exhibited elevated hydrogen deuterium exchange after peptide binding (Figure 9A–C).

The binding of the antibody to the CD20 peptide was quantified in more detail (Figure 10A,B). Early in the exchange reaction, the major contact point for the CD20 epitope peptide can be inferred to be CDR3 (V_H; *D* value = 0.574, peptide YYCVRASTGTSF). In the later time points, deuterium suppression is observed at both CDR2 domains; the *D* value for CDR2 (V_H) increases from −0.533 and 0.137, whilst the *D* value for CDR2 (V_L) increases from −0.232 to 0.150 (Figure 10B). CDR3 (V_L) interactions are not detected (Figure 10). The major sites exhibiting deuterium suppression late in the reaction are: (i) CDR2 (V_H) with a *D* value of 0.891; (ii) CDR2 (V_L) with a *D* values of being 0.608; and (iii) CDR3 (V_H) with a *D* value of 0.852. A summary of the deuteration mapping (Figure 11A) and the homology modelled variable domain (Figure 11B) highlights the regions whose deuteration is suppressed by peptide (in dark blue, CDR3 (V_H); in light blue, CDR2 (V_H), CDR2 (V_L), and CDR1 (V_L)) and those whose deuteration is increased (in red; CDR3,V_L).

We can propose an interpretation of these data. First, CDR3 (V_H) is the likely dominant paratope. In addition, the elevated deuteration in the Framework regions at later time points, as well as suppressed deuteration at the late time points in CDR2 regions, is suggestive of allosteric effects inducing conformational changes

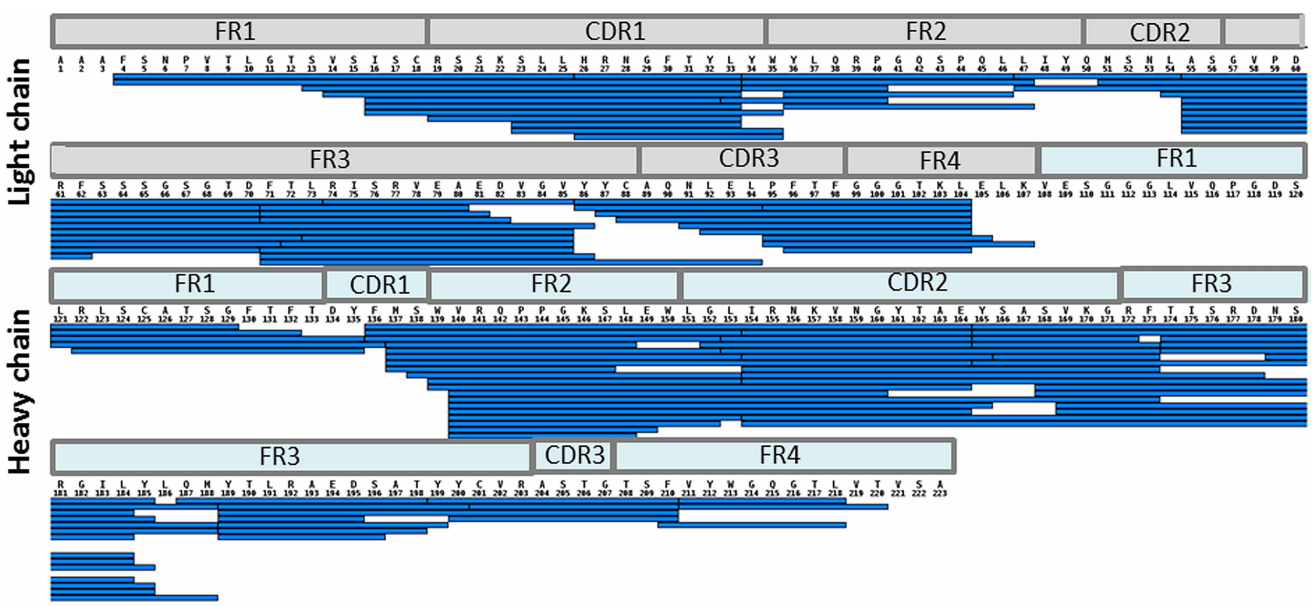

Figure 8. Proteolytic coverage of the NCD1.2 monoclonal antibody.

NCD1.2 IgG was processed after proteolytic digestion with pepsin and nepenthesin-1 followed by measurement using LC–MS/MS to identify the peptide coverage (91%) under conditions used for hydrogen deuterium exchange mass spectrometry (see Figure 9). Using MSTools [32], the blue boxes highlight coverage by 109 unique peptides with identified amino acid sequence of the antibody light and heavy chains. FR1 and CDR domains are marked as a function of the amino acid positions (the NCD1.2 has 223 amino acids).

Biochemical Journal (2021) **478** 99–120
https://doi.org/10.1042/BCJ20200674

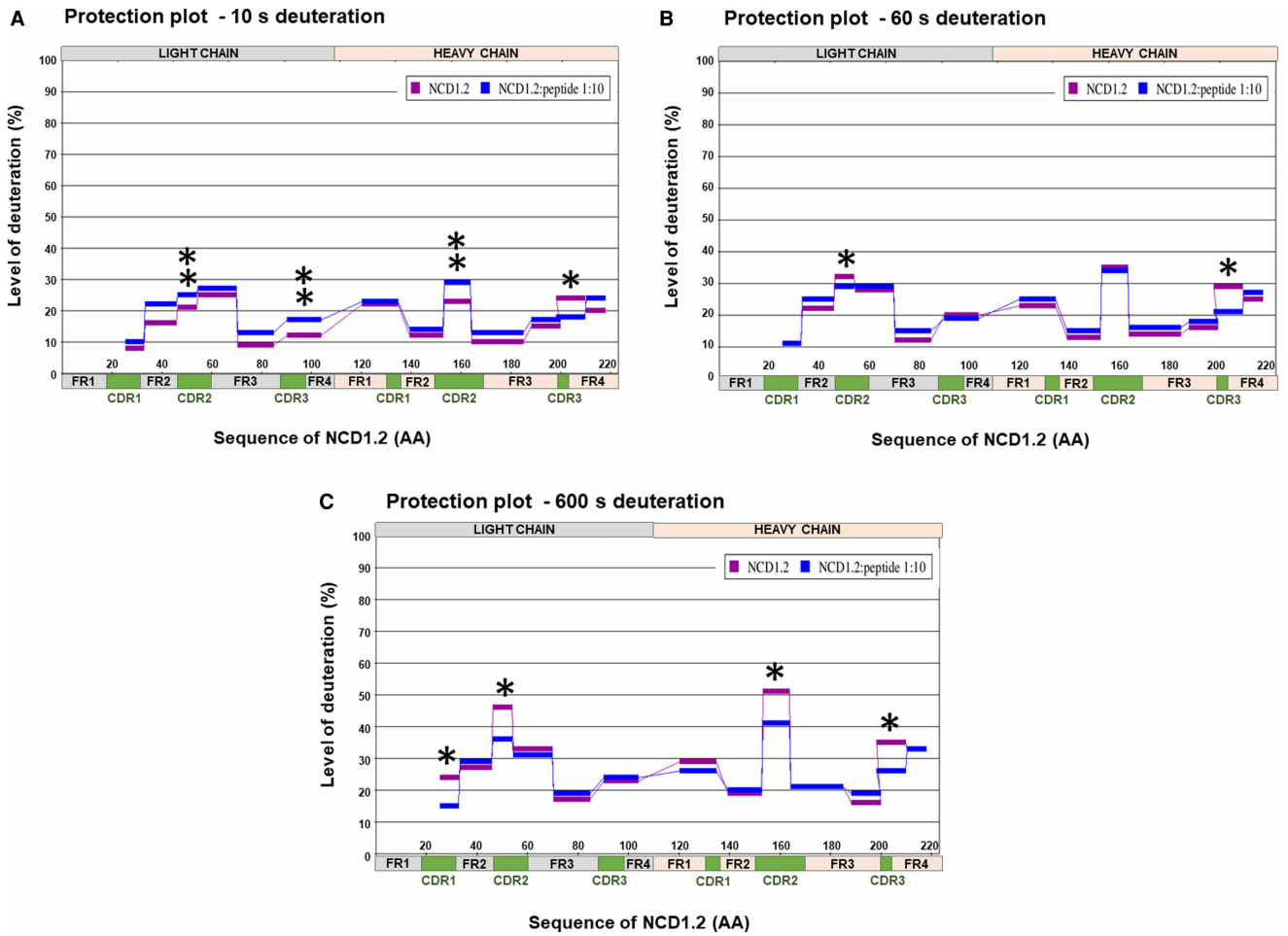

Figure 9. Kinetics of CD20 epitope binding by to NCD1.2 IgG.

The monoclonal antibody NCD1.2 (1 μM final concentration) was added to buffer in H_2O (75 mM Na_2HPO_4, 25 mM NaH_2PO_4, 50 mM KCl, pH 7.4) or the CD20 epitope peptide in a molar ratio 1: 10 (NCD1.2: CD20) and preincubated for 60 min at room temperature. Deuterium exchange was started by 10-fold dilution with buffer in D_2O with the same composition, pD 7.0 carried out at room temperature and quenched by acidification at the indicated time points (**A**) 10 s, (**B**) 1 min, and (**C**) 10 min. The samples were subjected to proteolysis and processed to measure using mass spectrometry changes in deuteration of the peptides as a function of time in the absence (blue) or presence (violet) of the CD20 peptide. The data are plotted as % deuteration of the peptide as a function of the numbering of the amino acids 1–221 (the peptides that were subjected to evaluation with HDExaminer software). The diagram highlights the positions of the CDR and FR domains from the light and heavy chain as a single polypeptide sequence of 221 amino acids for simplicity. Peptide deuteration is plotted directly above the CDR and FR domains for easy of comparison. The single asterisks highlight the CDR domains whose deuteration was suppressed by the CD20 peptide and the double asterisks highlight enhanced deuteration at the CDR domains.

including aggregation as well as local unfolding over the time course. For example, a prior study has shown that deuteration exchange-protected segments in the CDR domains of aggregated Bevacizumab likely represent intermolecular protein–protein interactions in ligand-induced aggregates [44].

To evaluate the quality and reproducibility of the methodology, we also prepared two alternative sets of the samples in triplicates: (i) one set at a molar ratio of 1 : 1 (antibody : peptide) incubated for 60 min at room temperature before the time course of deuteration and (ii) another set at a molar ratio 1 : 10 (antibody : peptide) without the 60 min pre-incubation of the peptide and antibody (Supplementary Figure S3). These experimental variations gave rise to data similar to that observed in Figure 9 (Supplementary Figure S3). The fact that deuterium uptake over the entire variable region of the IgG was nearly identical when there was no pre-incubation with antigen, or after a 60 min preincubation with antigen, also suggests that binding was established rapidly

Biochemical Journal (2021) **478** 99–120
https://doi.org/10.1042/BCJ20200674

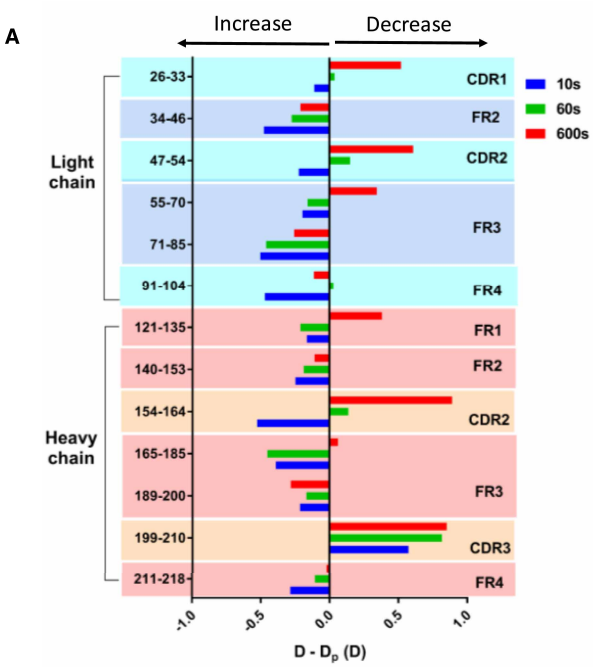

B

Peptides CD20 ScFv7		10 s			60 s			600 s		
		#D (S)	#D (S_p)	#D (S) - #D (S_p)	#D (S)	#D (S_p)	#D (S) - #D (S_p)	#D (S)	#D (S_p)	#D (S) - #D (S_p)
VYWGQGTL	211-218	1,213	1,498	**-0,285**	1,528	1,634	**-0,106**	2,002	2,023	**-0,021**
YYCVRASTGTSF	199-210	2,466	1,892	0,574	2,938	2,121	0,817	3,508	2,656	0,852
YTLRAEDSATYY	189-200	1,544	1,767	**-0,223**	1,638	1,814	**-0,176**	1,678	1,968	**-0,290**
YSASVKGRFTISRDNSRGILY	165-185	2,078	2,475	**-0,397**	2,736	3,194	**-0,458**	4,071	4,009	0,062
IRNKVNGYTAE	154-164	2,152	2,685	**-0,533**	3,200	3,063	0,137	4,650	3,759	0,891
VRQPPGKSLEWLGL	140-153	1,209	1,465	**-0,256**	1,396	1,592	**-0,196**	1,907	2,024	**-0,117**
LRLSCATSGFTFTDY	121-135	2,867	3,040	**-0,173**	3,065	3,285	**-0,220**	3,823	3,441	0,382
NLELPFTFGGGTKL	91-104	1,425	1,902	**-0,477**	2,204	2,175	**0,029**	2,539	2,662	**-0,123**
FTLRISRVEAEDVGV	71-85	1,189	1,698	**-0,509**	1,582	2,049	**-0,467**	2,257	2,522	**-0,265**
ASGVPDRFSSSGSGTD	55-70	3,322	3,527	**-0,205**	3,661	3,829	**-0,168**	4,407	4,063	0,344
LIYQMSNL	47-54	1,276	1,508	**-0,232**	1,943	1,793	0,150	2,809	2,201	0,608
YWYLQRPGQSPQL	34-46	1,506	1,990	**-0,484**	2,043	2,326	**-0,283**	2,451	2,671	**-0,220**
HRNGFTYL	26-33	0,494	0,613	**-0,119**	0,704	0,667	**0,037**	1,472	0,952	0,520

#D (S) is number of deuteria exchanged in peptides from CD20 ScFv antibody
#D (S_p) is number of deuteria exchanged in peptides from CD20 ScFv in complex with CD20 peptide

Figure 10. Quantitation of deuteration rates in NCD1.2 monoclonal antibody.

(**A**) A summary of the exchanged sites in the deuteration for the indicated peptides is plotted as a function of their position in the variable domain sequences from amino acids 26–218. Increased deuteration is a negative value whilst decreased deuteration is a positive value; *D*–*D*p is the difference between exchanged deuteria of the NCD1.2 ligand-free antibody(*D*) and NCD1.2 in complex with the CD20 antigen (*D*p). Deuteration without peptide–deuteration with peptide = *D*. The regions not interacting with the epitope peptide generally show elevated deuteration (negative *D*–*D*p (*D*) values), suggesting that the overall protein structure is 'open' or more flexible through an interaction with solvent in the presence of the CD20 epitope peptide. The data exported from *HDExaminer* are plotted for each peptide over the time course of 10, 60, or 600 s (early, intermediate, and late in the binding reaction). (**B**) The numerical *D*–*D*p = *D* data are summarized. Data used for the construction of deuteration graphs in part (**A**) was developed using GraphPad. Values of deuteria exchanged in peptides were exported from *HDExaminer*. Bold peptides and numbers highlight deprotected regions (elevated hydrogen exchanges with the deuterated solvent) of the NCD1.2 monoclonal antibody after CD20 binding at all measured time intervals. The regular case numbers are regions suppressed by deuteration.

after mixing of the monoclonal antibody and CD20 peptide. Rapid equilibration is also consistent with what would be expected given the rapid 'on' rates associated with most antibody/antigen interactions limited by diffusion [45].

Biochemical Journal (2021) **478** 99–120
https://doi.org/10.1042/BCJ20200674

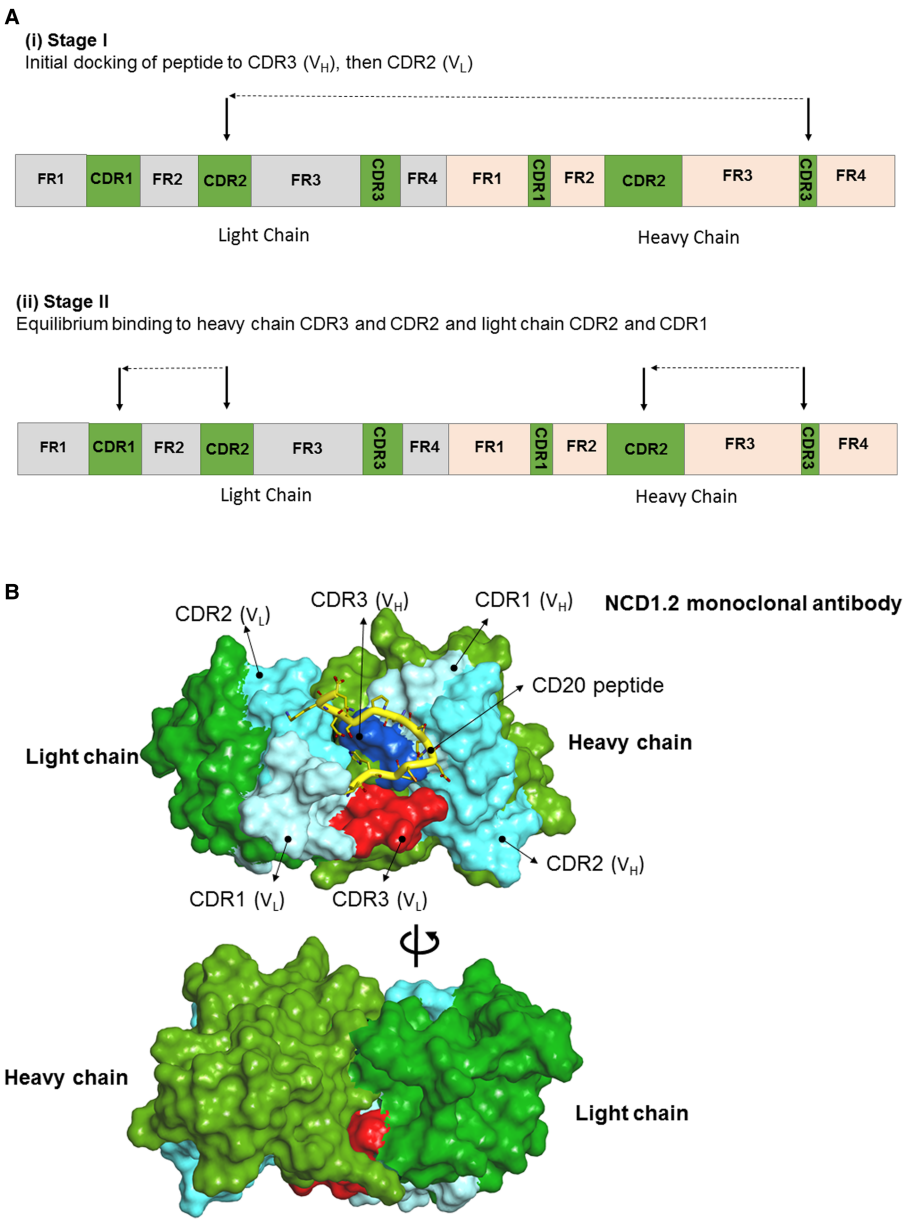

Figure 11. A summary of the dominant paratope involved in the antibody-peptide binding reaction. (**A**) (**i**) Early in the hydrogen deuterium exchange reaction, the major contact point for the CD20 epitope peptide is in CDR3 (V_H). (**ii**) In later time points, additional suppression occurs at CDR1 (V_H), CDR2 (V_H), CDR1 (V_L), and CDR2 (V_L)) as well as regions whose deuteration is increased in CDR3 (V_L). (**B**) The structural representation for the binding of the CD20 antigen with the NCD1.2 monoclonal antibody is shown in a space fill model. The right side of space fill models (front and back, 10 min deuteration) of the variable domains highlights the regions whose deuteration is suppressed by peptide; dark blue, CDR3 (V_H); in light blue, CDR1 (V_H), CDR2 (V_H), CDR1 (V_L), and CDR2 (V_L) and those whose deuteration is increased (in red scale; CDR3,V_L). Regions with no change in heavy chain and light chain are shown in green. These data together (from Figures 9 and 10) suggest that CDR3 (V_H) is the dominant binding site for the CD20 antigen; however, the suppression of hydrogen deuterium exchange at some of the additional CDR variable domains in parallel to increased hydrogen deuterium exchange at Framework domains suggests antigen-induced aggregation is occurring later in the reaction. The BIOVIA Discovery Studio (Dassault Systèmes, BIOVIA, San Diego, CA, U.S.A.) program, was used to visualize the 3D representation of the docked peptide-antibody structure/complex.

Biochemical Journal (2021) 478 99–120
https://doi.org/10.1042/BCJ20200674

Discussion

Canine and human B-cell lymphoma treatment undergo a chemotherapeutic regime termed CHOP; cyclophosphamide, hydroxydaunorubicin, oncovin, and prednisone. The addition of the anti-human CD20 antibody Rituximab increases disease-free survival rates in human patients [46]. This R-CHOP therapy is not available for canine lymphoma patients who only can access CHOP because Rituximab does not bind the canine CD20 epitope. In this report, we have characterized an anti-CD20 antibody named NCD1.2 that can bind canine CD20 [32]. This offers an opportunity to develop recombinant IgG suitable for use in veterinary medicine and also to develop more complex clinical trials to inform novel human treatments for lymphoma. However, an interesting feature of the NCD1.2 hybridoma is that it produces two variable light chain genes that potentially complicates the adaptation of this antibody as a therapeutic. Because hybridomas are not used as often as phage-antibody libraries, it is difficult to say how widespread this phenomenon might be. However, one study has shown that an anti-transferrin receptor antibody producing hybridoma cell produces three heavy-chains and three kappa (κ)-chain transcripts of which two light chains and one heavy chain were functional [47]. As such, it might not be unusual for a hybridoma to produce a complex IgG protein.

Because a mixed IgG chain would complicate or even preclude the development of a synthetic antibody based on NCD1.2 domain structure, the first aim of this report was to use mass spectrometry to determine the extent to which both light chains assemble into the full-length IgG. *De novo* protein sequencing of a protein typically can be performed using Edman degradation and/or mass spectrometry. Edman sequencing does not easily allow full sequence coverage and has more recently been used to sequence small regions of interest [48]. Mass spectrometry has emerged as a more robust tool, often in combination with Edman sequencing, with which to sequence proteins for which there is no reference dataset. A recent report highlighted the difficulty in acquiring full sequence coverage of an antibody using the Edman method [49]; this new method used protease XIII (*Aspergillus saitoi*) whilst electrospray voltage was applied to the digestion mixture through the emitter and Tandem MS data were captured as a function of proteolytic cleavage time.

More recently, two mass spectrometric approaches have been used to identify the sequence of a protein; bottom-up or top-down mass spectrometry. There are advantages and disadvantages to these collective methods. *De novo* antibody sequencing applying both a middle-down and top-down strategy used multiple ion activation stages to fragment and sequence the monoclonal antibody. Innovations in the bottom up method, have for example, applied the *Candida albicans* secreted aspartic protease Sap9 protease to enhance sequence coverage of peptides by producing larger peptides than trypsin, in the 3–5 kDa mass range [50]. The method described in our current study using NCD1.2 is described as 'bottom-up' approach that produces a peptide library that can be mapped onto a reference translated DNA sequence. Using this bottom-up mass spectrometric approach, combined with in-solution digestion of the NCD1.2 monoclonal antibody, we found that proteolysis either with trypsin or with trypsin and LysC were not successful in producing a high coverage of peptide fragments across the protein (data not shown). In contrast, the addition of Rapigest [44] to the NCD1.2 antibody, acidic conditions, and pepsin provided a 98% match of the amino acid sequence to the reference DNA sequence in one mass spectrometric run with using two fragmentation methods (CID and HCD). Using this bottom up method, we concluded that only one of the two light chains (Figure 1; Figure 3) predominates in the authentic hybridoma-derived full-length NCD1.2 IgG.

We then used hydrogen deuterium exchange mass spectrometry to identify the dominant paratope implicated in antigen binding. Hydrogen deuterium exchange mass spectrometry has been used previously to understand how a monoclonal antibody interacts with its antigen; for example, a monoclonal antibody that targets the Vaccinia virus L1 protein uses heavy chain CDR1 and CDR2 [51]. Hydrogen deuterium exchange mass spectrometry was used to identify oxidation states in CDR regions of a monoclonal antibody and infer action mechanism [52]. Using hydrogen deuterium exchange mass spectrometry on the anti-CD20 monoclonal antibody, there was one major feature observed (Figure 11A); suppression of CDR3 (V_H) deuteration in the presence of the CD20 antigen early in the exchange reaction (Figures 9A and 10A,B). In contrast, there was little interaction observed between the antigen and the light chain-7 CDR2(V_L) or CDR3 (V_L) (Figure 9A and 10A,B). These data suggest that CDR3 (V_H) forms the dominant docking site in the antigen-IgG. Future mutagenesis of the CDR3 (V_H) domain, the Fc domain, as well as 'canine-izing' the variable framework domains, might optimize the immunochemical properties of the recombinant NCD1.2 antibody. In addition, as complement mutants are emerging that might augment the human anti-CD20 monoclonal antibody [53], canine cancers might form a physiological preclinical testbed for translating such novel combined synthetic biologics for use in human lymphoma.

Biochemical Journal (2021) **478** 99–120
https://doi.org/10.1042/BCJ20200674

Competing Interests

The authors declare that there are no competing interests associated with the manuscript.

Funding

This work was supported in part by the BBSRC UK (BB/J00751X/1; BBSRC IAA, TEC3706; BBSRC IAA PIII-024, BB/R012385/1 (pathfinder)), by the European Regional Development Fund — Project ENOCH (No. CZ.02.1.01/0.0/0.0/16_019/0000868), by the Ministry of Health Development of Research Organization, MH CZ — DRO (MMCI, 00209805) and by The International Centre for Cancer Vaccine Science, a project is carried out within the International Research Agendas programme of the Foundation for Polish Science co-financed by the European Union under the European Regional Development Fund. MN was supported by Czech Science Foundation project number 18-23773Y. P.M. was supported by grant AZV NV18-03-00339.

CRediT Contribution

Lenka Hernychova: Investigation, Methodology, Writing — original draft, Writing — review and editing. **Lukas Uhrik**: Data curation, Investigation. **Petr Muller**: Resources, Validation. **Umesh Kalathiya**: Formal analysis, Visualization. **Malgorzata M. Lisowska**: Resources, Methodology. **Mikolaj Kocikowski**: Resources, Visualization. **Maciej Parys**: Resources, Data curation. **Jakub Faktor**: Data curation, Writing — original draft. **Marta Nekulova**: Validation, Visualization. **Chris Nortcliffe**: Data curation. **Pavlina Zatloukalova**: Data curation, Visualization. **Barbara Ruetgen**: Supervision, Validation, Visualization, Project administration. **Robin Fahraeus**: Supervision, Project administration. **Kathryn L. Ball**: Supervision, Funding acquisition, Project administration. **David J. Argyle**: Supervision, Funding acquisition, Project administration, Writing — review and editing. **Borivoj Vojtesek**: Conceptualization, Supervision, Funding acquisition, Writing — original draft, Writing — review and editing. **Ted Hupp**: Conceptualization, Supervision, Funding acquisition, Validation, Visualization, Writing — original draft.

Abbreviations

ACN, acetonitrile; ADCC, antibody-dependent cell-mediated cytotoxicity; ADCP, antibody-dependent cell-mediated phagocytosis; CD, cluster of differentiation; CDC, complement-dependent cytotoxicity; CDR, complementarity-determining regions; CID, collision-induced dissociation; CTLA-4, cytotoxic T-lymphocyte antigen 4; ERBB2, erb-b2 receptor tyrosine kinase 2; FA, formic acid; FAM, 6-carboxyfluorescein (6-FAM); Fc, fragment crystallizable region; FcR, Fc receptor; FDR, false discovery rate; FR, framework region; HCD, higher-energy collisional dissociation; HDX, hydrogen deuterium exchange; IDA, information-dependent mode; IgG, immunoglobulin G; LC–MS/MS, liquid chromatography–tandem mass spectrometry; MS, mass spectrometry; NK, natural killer; PD1, programmed cell death; PDL1, programmed death-ligand 1; scFV, single-chain variable fragment; TCEP, tris(2-carboxyethyl)phosphine hydrochloride; TFA, trifluoroacetic acid; VEGF, vascular endothelial growth factor; VEGFR, vascular endothelial growth factor receptor.

References

1 Hanahan, D. and Weinberg, R.A. (2011) Hallmarks of cancer: the next generation. *Cell* **144**, 646–674 https://doi.org/10.1016/j.cell.2011.02.013
2 van Helden, P.D., van Helden, L.S. and Hoal, E.G. (2013) One world, one health. Humans, animals and the environment are inextricably linked–a fact that needs to be remembered and exploited in our modern approach to health. *EMBO Rep.* **14**, 497–501 https://doi.org/10.1038/embor.2013.61
3 Alirol, E., Getaz, L., Stoll, B., Chappuis, F. and Loutan, L. (2011) Urbanisation and infectious diseases in a globalised world. *Lancet Infect. Dis.* **11**, 131–141 https://doi.org/10.1016/S1473-3099(10)70223-1
4 Morcos, P.N., Boehnke, A., Valente, N. and Mager, D.E. (2019) Rituximab dosing in hematological malignancies: an old question, revisited. *Cancer Chemother. Pharmacol.* **84**, 661–666 https://doi.org/10.1007/s00280-019-03818-1
5 Ingles Garces, A.H., Au, L., Mason, R., Thomas, J. and Larkin, J. (2019) Building on the anti-PD1/PD-L1 backbone: combination immunotherapy for cancer. *Exp. Opin. Invest. Drugs* **28**, 695–708 https://doi.org/10.1080/13543784.2019.1649657
6 Van Allen, E.M., Miao, D., Schilling, B., Shukla, S.A., Blank, C., Zimmer, L. et al. (2015) Genomic correlates of response to CTLA-4 blockade in metastatic melanoma. *Science* **350**, 207–211 https://doi.org/10.1126/science.aad0095
7 Scott, A.M., Wolchok, J.D. and Old, L.J. (2012) Antibody therapy of cancer. *Nat. Rev. Cancer* **12**, 278–287 https://doi.org/10.1038/nrc3236
8 Bakacs, T., Mehrishi, J.N. and Moss, R.W. (2012) Ipilimumab (Yervoy) and the TGN1412 catastrophe. *Immunobiology* **217**, 583–589 https://doi.org/10.1016/j.imbio.2011.07.005
9 Fares, C.M., Van Allen, E.M., Drake, C.G., Allison, J.P. and Hu-Lieskovan, S. (2019) Mechanisms of resistance to immune checkpoint blockade: why does checkpoint inhibitor immunotherapy not work for all patients? *Am. Soc. Clin. Oncol. Educ. Book* **39**, 147–164 https://doi.org/10.1200/EDBK_240837
10 Khanna, C., Lindblad-Toh, K., Vail, D., London, C., Bergman, P., Barber, L. et al. (2006) The dog as a cancer model. *Nat. Biotechnol.* **24**, 1065–1066 https://doi.org/10.1038/nbt0906-1065b

11 Shao, Y.W., Wood, G.A., Lu, J., Tang, Q.L., Liu, J., Molyneux, S. et al. (2019) Cross-species genomics identifies DLG2 as a tumor suppressor in osteosarcoma. *Oncogene* **38**, 291–298 https://doi.org/10.1038/s41388-018-0444-4
12 Diessner, B.J., Marko, T.A., Scott, R.M., Eckert, A.L., Stuebner, K.M., Hohenhaus, A.E. et al. (2019) A comparison of risk factors for metastasis at diagnosis in humans and dogs with osteosarcoma. *Cancer Med.* **8**, 3216–3226 https://doi.org/10.1002/cam4.2177
13 Fazekas-Singer, J., Berroteran-Infante, N., Rami-Mark, C., Dumanic, M., Matz, M., Willmann, M. et al. (2017) Development of a radiolabeled caninized anti-EGFR antibody for comparative oncology trials. *Oncotarget* **8**, 83128–83141 https://doi.org/10.18632/oncotarget.20914
14 Singer, J., Fazekas, J., Wang, W., Weichselbaumer, M., Matz, M., Mader, A. et al. (2014) Generation of a canine anti-EGFR (ErbB-1) antibody for passive immunotherapy in dog cancer patients. *Mol. Cancer Ther.* **13**, 1777–1790 https://doi.org/10.1158/1535-7163.MCT-13-0288
15 Amin, S.B., Anderson, K.J., Boudreau, C.E., Martinez-Ledesma, E., Kocakavuk, E., Johnson, K.C. et al. (2020) Comparative molecular life history of spontaneous canine and human gliomas. *Cancer Cell* **37**, 243–257.e247 https://doi.org/10.1016/j.ccell.2020.01.004
16 MacDiarmid, J.A., Langova, V., Bailey, D., Pattison, S.T., Pattison, S.L., Christensen, N. et al. (2016) Targeted doxorubicin delivery to brain tumors via minicells: proof of principle using dogs with spontaneously occurring tumors as a model. *PLoS One* **11**, e0151832 https://doi.org/10.1371/journal.pone.0151832
17 Perosa, F., Favoino, E., Caragnano, M.A., Prete, M. and Dammacco, F. (2005) CD20: a target antigen for immunotherapy of autoimmune diseases. *Autoimmun. Rev.* **4**, 526–531 https://doi.org/10.1016/j.autrev.2005.04.004
18 Ernst, J.A., Li, H., Kim, H.S., Nakamura, G.R., Yansura, D.G. and Vandlen, R.L. (2005) Isolation and characterization of the B-cell marker CD20. *Biochemistry* **44**, 15150–15158 https://doi.org/10.1021/bi0511078
19 Griffin, M.M. and Morley, N. (2013) Rituximab in the treatment of non-Hodgkin's lymphoma–a critical evaluation of randomized controlled trials. *Exp. Opin. Biol. Ther.* **13**, 803–811 https://doi.org/10.1517/14712598.2013.786698
20 Maloney, D.G., Grillo-Lopez, A.J., White, C.A., Bodkin, D., Schilder, R.J., Neidhart, J.A. et al. (1997) IDEC-C2B8 (Rituximab) anti-CD20 monoclonal antibody therapy in patients with relapsed low-grade non-Hodgkin's lymphoma. *Blood* **90**, 2188–2195 https://doi.org/10.1182/blood.V90.6.2188
21 Chambers, S.A. and Isenberg, D. (2005) Anti-B cell therapy (rituximab) in the treatment of autoimmune diseases. *Lupus* **14**, 210–214 https://doi.org/10.1191/0961203305lu2138oa
22 Sinha, A. and Bagga, A. (2013) Rituximab therapy in nephrotic syndrome: implications for patients' management. *Nat. Rev. Nephrol.* **9**, 154–169 https://doi.org/10.1038/nrneph.2012.289
23 Lee, S. and Ballow, M. (2010) Monoclonal antibodies and fusion proteins and their complications: targeting B cells in autoimmune diseases. *J. Allergy Clin. Immunol.* **125**, 814–820 https://doi.org/10.1016/j.jaci.2010.02.025
24 Castillo-Trivino, T., Braithwaite, D., Bacchetti, P. and Waubant, E. (2013) Rituximab in relapsing and progressive forms of multiple sclerosis: a systematic review. *PLoS One* **8**, e66308 https://doi.org/10.1371/journal.pone.0066308
25 Vo, A.A., Choi, J., Cisneros, K., Reinsmoen, N., Haas, M., Ge, S. et al. (2014) Benefits of rituximab combined with intravenous immunoglobulin for desensitization in kidney transplant recipients. *Transplantation* **98**, 312–319 https://doi.org/10.1097/TP.0000000000000064
26 Vital, E.M., Kay, J. and Emery, P. (2013) Rituximab biosimilars. *Exp. Opin. Biol. Ther.* **13**, 1049–1062 https://doi.org/10.1517/14712598.2013.787064
27 Pouget, J.P., Navarro-Teulon, I., Bardies, M., Chouin, N., Cartron, G., Pelegrin, A. et al. (2011) Clinical radioimmunotherapy–the role of radiobiology. *Nat. Rev. Clin. Oncol.* **8**, 720–734 https://doi.org/10.1038/nrclinonc.2011.160
28 Wiseman, G.A., Gordon, L.I., Multani, P.S., Witzig, T.E., Spies, S., Bartlett, N.L. et al. (2002) Ibritumomab tiuxetan radioimmunotherapy for patients with relapsed or refractory non-Hodgkin lymphoma and mild thrombocytopenia: a phase II multicenter trial. *Blood* **99**, 4336–4342 https://doi.org/10.1182/blood.V99.12.4336
29 Kasi, P.M., Tawbi, H.A., Oddis, C.V. and Kulkarni, H.S. (2012) Clinical review: Serious adverse events associated with the use of rituximab - a critical care perspective. *Crit. Care* **16**, 231 https://doi.org/10.1186/cc11304
30 Mudaliar, M.A., Haggart, R.D., Miele, G., Sellar, G., Tan, K.A., Goodlad, J.R. et al. (2013) Comparative gene expression profiling identifies common molecular signatures of NF-kappaB activation in canine and human diffuse large B cell lymphoma (DLBCL). *PLoS One* **8**, e72591 https://doi.org/10.1371/journal.pone.0072591
31 Argyle, D.J. and Pecceu, E. (2016) Canine and feline lymphoma: challenges and opportunities for creating a paradigm shift. *Vet. Comp. Oncol.* **14**, 1–7 https://doi.org/10.1111/vco.12253
32 Jain, S., Aresu, L., Comazzi, S., Shi, J., Worrall, E., Clayton, J. et al. (2016) The development of a recombinant scFv monoclonal antibody targeting canine CD20 for use in comparative medicine. *PLoS One* **11**, e0148366 https://doi.org/10.1371/journal.pone.0148366
33 Ito, D., Brewer, S., Modiano, J.F. and Beall, M.J. (2015) Development of a novel anti-canine CD20 monoclonal antibody with diagnostic and therapeutic potential. *Leuk. Lymphoma* **56**, 219–225 https://doi.org/10.3109/10428194.2014.914193
34 Rutgen, B.C., Willenbrock, S., Reimann-Berg, N., Walter, I., Fuchs-Baumgartinger, A., Wagner, S. et al. (2012) Authentication of primordial characteristics of the CLBL-1 cell line prove the integrity of a canine B-cell lymphoma in a murine in vivo model. *PLoS One* **7**, e40078 https://doi.org/10.1371/journal.pone.0040078
35 Masson, G.R., Burke, J.E., Ahn, N.G., Anand, G.S., Borchers, C., Brier, S. et al. (2019) Recommendations for performing, interpreting and reporting hydrogen deuterium exchange mass spectrometry (HDX-MS) experiments. *Nat. Methods* **16**, 595–602 https://doi.org/10.1038/s41592-019-0459-y
36 Kavan, D. and M, P. (2011) MSTools-Web based application for visualization and presentation of HXMS data. *Int. J. Mass Spectrom.* **302**, 53–58 https://doi.org/10.1016/j.ijms.2010.07.030
37 Perez-Riverol, Y., Csordas, A., Bai, J., Bernal-Llinares, M., Hewapathirana, S., Kundu, D.J. et al. (2019) The PRIDE database and related tools and resources in 2019: improving support for quantification data. *Nucleic Acids Res.* **47**, D442–D450 https://doi.org/10.1093/nar/gky1106
38 Islam, M.T., Mohamedali, A., Fernandes, C.S., Baker, M.S. and Ranganathan, S. (2017) De novo peptide sequencing: deep mining of high-Resolution mass spectrometry data. *Methods Mol. Biol.* **1549**, 119–134 https://doi.org/10.1007/978-1-4939-6740-7_10
39 Fornelli, L., Srzentic, K., Huguet, R., Mullen, C., Sharma, S., Zabrouskov, V. et al. (2018) Accurate sequence analysis of a monoclonal antibody by top-down and middle-down orbitrap mass spectrometry applying multiple Ion activation techniques. *Anal. Chem.* **90**, 8421–8429 https://doi.org/10.1021/acs.analchem.8b00984
40 Tang, L., Sampson, C., Dreitz, M.J. and McCall, C. (2001) Cloning and characterization of cDNAs encoding four different canine immunoglobulin gamma chains. *Vet. Immunol. Immunopathol.* **80**, 259–270 https://doi.org/10.1016/S0165-2427(01)00318-X

Biochemical Journal (2021) **478** 99–120
https://doi.org/10.1042/BCJ20200674

41 Teeling, J.L., Mackus, W.J., Wiegman, L.J., van den Brakel, J.H., Beers, S.A., French, R.R. et al. (2006) The biological activity of human CD20 monoclonal antibodies is linked to unique epitopes on CD20. *J. Immunol.* **177**, 362–371 https://doi.org/10.4049/jimmunol.177.1.362

42 Unruh, T.L., Zuccolo, J., Beers, S.A., Kanevets, U., Shi, Y. and Deans, J.P. (2010) Therapeutic (high) doses of rituximab activate calcium mobilization and inhibit B-cell growth via an unusual mechanism triggered independently of both CD20 and Fcgamma receptors. *J. Immunother.* **33**, 30–39 https://doi.org/10.1097/CJI.0b013e3181b290f1

43 Berkman, P., Vardinon, N. and Yust, I. (2002) Antibody dependent cell mediated cytotoxicity and phagocytosis of senescent erythrocytes by autologous peripheral blood mononuclear cells. *Autoimmunity* **35**, 415–419 https://doi.org/10.1080/0891693021000005394

44 Kheterpal, I., Cook, K.D. and Wetzel, R. (2006) Hydrogen/deuterium exchange mass spectrometry analysis of protein aggregates. *Methods Enzymol.* **413**, 140–166 https://doi.org/10.1016/S0076-6879(06)13008-6

45 Galanti, M., Fanelli, D. and Piazza, F. (2016) Conformation-controlled binding kinetics of antibodies. *Sci. Rep.* **6**, 18976 https://doi.org/10.1038/srep18976

46 Coiffier, B., Lepage, E., Briere, J., Herbrecht, R., Tilly, H., Bouabdallah, R. et al. (2002) CHOP chemotherapy plus rituximab compared with CHOP alone in elderly patients with diffuse large-B-cell lymphoma. *N. Engl. J. Med.* **346**, 235–242 https://doi.org/10.1056/NEJMoa011795

47 Yang, J., Zhu, H., Tan, Z., He, F., Sun, X., Hong, Y. et al. (2013) Comparison of two functional kappa light-chain transcripts amplified from a hybridoma. *Biotechnol. Appl. Biochem.* **60**, 289–297 https://doi.org/10.1002/bab.1080

48 Zhang, B., Yang, Y., Yuk, I., Pai, R., McKay, P., Eigenbrot, C. et al. (2008) Unveiling a glycation hot spot in a recombinant humanized monoclonal antibody. *Anal. Chem.* **80**, 2379–2390 https://doi.org/10.1021/ac701810q

49 Mao, Y., Zhang, L., Kleinberg, A., Xia, Q., Daly, T.J. and Li, N. (2019) Fast protein sequencing of monoclonal antibody by real-time digestion on emitter during nanoelectrospray. *Monoclon. Antibodies* **11**, 767–778 https://doi.org/10.1080/19420862.2019.1599633

50 Laskay, U.A., Srzentic, K., Monod, M. and Tsybin, Y.O. (2014) Extended bottom-up proteomics with secreted aspartic protease Sap9. *J. Proteomics* **110**, 20–31 https://doi.org/10.1016/j.jprot.2014.07.035

51 Kaever, T., Meng, X., Matho, M.H., Schlossman, A., Li, S., Sela-Culang, I. et al. (2014) Potent neutralization of vaccinia virus by divergent murine antibodies targeting a common site of vulnerability in L1 protein. *J. Virol.* **88**, 11339–11355 https://doi.org/10.1128/JVI.01491-14

52 Yan, Y., Wei, H., Fu, Y., Jusuf, S., Zeng, M., Ludwig, R. et al. (2016) Isomerization and oxidation in the complementarity-Determining regions of a monoclonal antibody: a study of the modification-structure-function correlations by hydrogen-dDeuterium exchange mass spectrometry. *Anal. Chem.* **88**, 2041–2050 https://doi.org/10.1021/acs.analchem.5b02800

53 Felberg, A., Urban, A., Borowska, A., Stasilojc, G., Taszner, M., Hellmann, A. et al. (2019) Mutations resulting in the formation of hyperactive complement convertases support cytocidal effect of anti-CD20 immunotherapeutics. *Cancer Immunol. Immunother.* **68**, 587–598 https://doi.org/10.1007/s00262-019-02304-0